Journal of Positive Sciences (JPS) eISSN: 2582-9351, https://positive-sciences.com JPS. 2026 May; 6(3): 101-125

Article info
Received on: 05.04.2026
Accepted on: 23.05.2026
Published on: 26.05.2026
doi: https://doi.org/10.52688/ASP13650

Research Article

Comparative Study on the Mechanical Improvement of Aluminum Piston Alloys

Haitham Mohammed Ibrahim Al-Zuhairi [1], Iqbal alshalal [2], Hind H. Abbood [3], Mohammed RASHEED [4, *]

[1, 2, 3] Training and Workshop Center, University of Technology- Iraq, Baghdad, Iraq
[4] Production Engineering & Metallurgy College, University of Technology- Iraq, Baghdad 10066, Iraq

[*] rasheed.mohammed40@yahoo.com

ABSTRACT

Aluminum piston alloys are extensively employed in automotive engines because of their low density, excellent thermal conductivity, good castability, and favorable strength-to-weight ratio. However, repeated thermal fluctuations and cyclic mechanical loading during engine operation can accelerate crack initiation, reduce fatigue life, and compromise long-term reliability. The present study comparatively investigates the effect of different heat-treatment conditions on the structural and mechanical performance of aluminum piston alloys. Four representative conditions were considered: as-cast alloy (S1), solution-treated alloy (S2), T6-treated alloy consisting of solution treatment followed by artificial aging (S3), and over-aged alloy (S4). Optical microscopy, SEM/EDS, XRD, and FESEM analyses were employed to correlate microstructural evolution with mechanical behavior. XRD results revealed that the average crystallite size increased from 28.05 nm for S1 to 31.00 nm for S2 and reached 37.27 nm for S3 before decreasing to 32.12 nm in S4. Concurrently, the microstrain decreased from 2.63–4.89 × 10^{-3} in S1 to 1.93–3.81 × 10^{-3} in S3, accompanied by a reduction in dislocation density from 1.17–1.39 × 10^{-3} nm^{-2} to 0.66–0.78 × 10^{-3} nm^{-2}. Tensile testing showed that the yield strength increased from 128 MPa in S1 to 182 MPa in S3, while the ultimate tensile strength improved from 185 MPa to 265 MPa, and elongation increased from 4.8% to 7.1%. The impact strength rose from 85 kJ/m^2 to 134 kJ/m^2, whereas the fatigue life increased markedly from 1.2 × 10^5 cycles to 6.8 × 10^5 cycles after T6 treatment. FESEM fractography revealed a transition from brittle cleavage fracture in the as-cast alloy to ductile microvoid coalescence in the T6-treated condition. These findings demonstrate that controlled thermal processing, particularly T6 treatment, effectively tailors the microstructure of aluminum piston alloys to achieve enhanced strength, toughness, and resistance to cyclic loading, making such alloys highly suitable for advanced automotive piston applications.

KEYWORDS: Aluminum piston alloys; heat treatment; T6 aging; XRD; tensile properties; impact strength; fatigue behavior; FESEM fractography

INTRODUCTION

Aluminum piston alloys have become indispensable materials in modern automotive engines owing to their low density, excellent thermal conductivity, high specific strength, and superior castability [1]. Compared with conventional ferrous materials, aluminum alloys significantly reduce the overall weight of engine components, contributing to improved fuel efficiency, lower emissions, and enhanced vehicle performance [2]. Among various applications, pistons are subjected to some of the most severe operating conditions, including elevated temperatures, cyclic mechanical loading, frictional wear, and thermal fluctuations [3]. Consequently, maintaining the mechanical integrity and dimensional stability of piston materials during prolonged service remains a major challenge [4]. Hypoeutectic and eutectic Al–Si alloys are widely utilized in piston manufacturing due to their favorable combination of wear resistance and thermal properties [5].

*Corresponding author
Mohammed RASHEED,
Production Engineering & Metallurgy College, University of Technology- Iraq, Baghdad 10066, Iraq
e-mail: rasheed.mohammed40@yahoo.com

Nevertheless, the as-cast microstructure of these alloys often contains coarse silicon particles, non-uniform intermetallic compounds, and residual stresses that adversely affect mechanical properties such as hardness, tensile strength, fatigue resistance, and impact toughness. These microstructural imperfections may accelerate crack initiation and propagation, ultimately reducing component reliability [6].

Heat treatment is one of the most effective and economically feasible approaches for enhancing the performance of aluminum piston alloys. Solution treatment promotes the dissolution of soluble alloying phases and homogenizes the matrix composition, while artificial aging induces the precipitation of fine strengthening phases that impede dislocation movement [7]. The resulting precipitation hardening mechanism substantially improves hardness and strength without significantly increasing component weight. The T6 heat-treatment condition, involving solution treatment followed by artificial aging, has been extensively employed to optimize the balance between strength and ductility in Al–Si piston alloys. Conversely, excessive aging may lead to precipitate coarsening and over-aging, reducing the strengthening effect and deteriorating fatigue performance. Therefore, understanding the relationship between heat-treatment conditions, microstructural evolution, and mechanical behavior is essential for selecting suitable processing parameters for high-performance piston applications [8].

Despite the widespread industrial use of aluminum piston alloys, premature failures associated with fatigue cracking, wear, and thermal degradation continue to occur under demanding engine operating conditions. Many commercially used alloys are employed in the as-cast condition or under non-optimized thermal processing schedules, leading to inconsistent mechanical performance. Although heat treatment has been recognized as a promising strategy for property enhancement, a comprehensive comparison of different thermal conditions and their corresponding effects on multiple mechanical characteristics remains limited. Consequently, there is a need for a systematic investigation to determine the most effective treatment condition capable of maximizing the overall performance of aluminum piston alloys.

Previous studies have primarily focused on individual mechanical properties such as hardness or tensile strength, often neglecting other critical aspects including fatigue resistance, impact behavior, and wear performance. Moreover, many investigations have evaluated only one or two heat-treatment conditions without establishing a direct comparative relationship among various processing states. The lack of an integrated understanding of how thermal treatments simultaneously influence microstructure and multiple mechanical responses represents a significant knowledge gap.

The motivation of this study arises from the increasing demand for lightweight, durable, and energy-efficient automotive components. Improving piston alloy performance through optimized heat treatment can contribute to longer service life, enhanced engine reliability, and reduced maintenance costs. Therefore, a comparative study addressing these limitations is both scientifically valuable and industrially relevant.

The primary objective of this study is to perform a comprehensive comparative evaluation of the mechanical improvement of aluminum piston alloys subjected to different heat-treatment conditions commonly employed in automotive applications. Particular emphasis is placed on understanding how thermal processing influences the microstructural evolution of the alloy and how these changes affect its overall mechanical performance. To achieve this objective, the study investigates the relationship between heat-treatment-induced microstructural modifications and key mechanical properties, including hardness, tensile strength, impact toughness, wear resistance, and fatigue behavior. By systematically comparing the responses of the investigated samples, the work aims to identify the treatment condition that offers the most favorable balance between strength, durability, and reliability required for piston service under severe operating conditions. In addition, the findings are intended to provide practical guidance for selecting appropriate thermal processing routes in the manufacturing of high-performance aluminum pistons for modern automotive engines. The scope of this investigation is limited to four representative processing conditions, namely the as-cast alloy (S1), solution-treated alloy (S2), solution-treated and artificially aged alloy (S3), and over-aged alloy (S4). The study focuses exclusively on the effects of thermal treatments on the mechanical characteristics of aluminum piston alloys and does not consider other enhancement approaches such as compositional modifications, reinforcement additions, or surface engineering techniques.

The novelty of the present study resides in its comprehensive and systematic comparative evaluation of aluminum piston alloys subjected to four distinct thermal processing conditions within a unified experimental framework. While previous investigations have predominantly focused on the influence of heat treatment on individual properties, such as hardness or tensile strength, the current work provides an

*Corresponding author
Mohammed RASHEED,
Production Engineering & Metallurgy College, University of Technology- Iraq, Baghdad 10066, Iraq
e-mail: rasheed.mohammed40@yahoo.com

integrated assessment of the combined effects of thermal processing on microstructural evolution and a broad spectrum of mechanical characteristics. Specifically, the study simultaneously examines hardness, tensile behavior, impact toughness, wear resistance, and fatigue performance, thereby offering a more holistic understanding of the structure–property relationships governing the performance of aluminum piston alloys. By directly comparing the as-cast (S1), solution-treated (S2), solution-treated and artificially aged (T6) (S3), and over-aged (S4) conditions, this research identifies the processing route that delivers the optimum balance between strength, toughness, durability, and service reliability. Furthermore, the study establishes clear correlations between heat-treatment-induced microstructural modifications and the resulting mechanical responses, providing valuable insights into the mechanisms responsible for performance enhancement. The findings contribute practical recommendations for improving the operational efficiency and lifespan of aluminum pistons used in automotive engines and generate a comprehensive experimental dataset that can serve as a useful reference for future alloy development, thermal processing optimization, and the design of advanced lightweight engine materials.

Although the present study provides valuable insights into the mechanical improvement of aluminum piston alloys, several limitations should be acknowledged. First, the investigation is restricted to a single piston alloy composition and may not fully represent the behavior of all commercial aluminum alloys. Second, the study considers only thermal processing as the enhancement technique and does not examine alternative methods such as nanoparticle reinforcement, surface modification, or severe plastic deformation. Third, the experimental conditions employed in laboratory testing cannot entirely replicate the complex thermo-mechanical environment encountered during actual engine operation. Finally, long-term creep behavior and corrosion performance were not evaluated and may be considered in future studies.

The remainder of this paper is organized as follows. Section 2 describes the materials, sample preparation procedures, heat-treatment schedules, and experimental techniques used for microstructural characterization and mechanical testing. Section 3 presents and discusses the results obtained from microstructural observations and the evaluation of hardness, tensile properties, impact resistance, wear characteristics, and fatigue behavior under different treatment conditions. Finally, Section 4 summarizes the major findings of the study, highlights the practical implications of the results, and proposes recommendations for future research aimed at further improving the performance of aluminum piston alloys.

MATERIALS AND METHODS

SAMPLE PREPARATION (S1–S4)

Commercial aluminum piston alloy ingots were used as the starting material in this investigation. The chemical composition of the alloy was selected to represent conventional Al–Si piston alloys widely employed in automotive engine applications because of their favorable combination of low density, high thermal conductivity, good castability, and excellent wear resistance. The alloy was melted in an electric resistance furnace at a temperature of approximately 750 ± 10 °C and stirred to ensure chemical homogeneity. The molten metal was subsequently poured into a preheated permanent steel mold to produce cylindrical castings suitable for specimen fabrication. After solidification and cooling to room temperature, the castings were machined according to the dimensions required for the various characterization and mechanical testing procedures.

To evaluate the influence of thermal processing on the mechanical performance of the piston alloy, four representative sample conditions were prepared. The first condition, designated as S1, corresponded to the as-cast alloy, which served as the reference sample without any post-casting thermal treatment. The second condition, S2, consisted of the solution-treated alloy, in which the machined specimens were heated at 520 °C for 6 h to dissolve soluble phases and homogenize the microstructure, followed by rapid quenching in water at room temperature. The third condition, S3, represented the solution-treated and artificially aged (T6) alloy. After solution treatment and quenching, the specimens were artificially aged at 175 °C for 8 h and then allowed to cool in air. This treatment was intended to promote the formation of fine and uniformly distributed strengthening precipitates within the aluminum matrix. The fourth condition, designated as S4, corresponded to the over-aged alloy, in which the solution-treated specimens were aged at 250 °C for 10 h to induce precipitate coarsening and evaluate its effect on the mechanical behavior of the alloy.

*Corresponding author
Mohammed RASHEED,
Production Engineering & Metallurgy College, University of Technology- Iraq, Baghdad 10066, Iraq
e-mail: rasheed.mohammed40@yahoo.com

The preparation route adopted in this study enabled a direct comparison of the effects of different heat-treatment conditions on the microstructural evolution and mechanical characteristics of aluminum piston alloys. The selected thermal schedules were based on commonly reported industrial practices for Al–Si piston materials and were chosen to represent the major stages of precipitation hardening, ranging from the untreated state to the over-aged condition. The designation and processing conditions of the investigated samples are summarized in Table 1.

Table 1. Sample designation and thermal processing conditions of the investigated aluminum piston alloys.

Sample	Condition	Heat-Treatment Parameters	Cooling Method
S1	As-cast alloy	No heat treatment	Air cooling
S2	Solution-treated alloy	520 °C for 6 h	Water quenching
S3	T6-treated alloy	520 °C for 6 h + 175 °C for 8 h	Water quenching + air cooling
S4	Over-aged alloy	520 °C for 6 h + 250 °C for 10 h	Water quenching + air cooling

All specimens prepared under these conditions were subsequently subjected to microstructural characterization and mechanical testing to establish the relationship between thermal processing, microstructural development, and mechanical performance

EXPERIMENTAL PROCEDURES

The experimental procedures employed in this study were designed to systematically evaluate the influence of different heat-treatment conditions on the microstructural characteristics and mechanical performance of aluminum piston alloys. Following sample preparation and thermal processing, the specimens were subjected to a series of characterization techniques and standardized mechanical tests to establish correlations between microstructural evolution and the resulting mechanical behavior. For microstructural examination, metallographic specimens obtained from each sample condition (S1–S4) were sectioned using a precision cutting machine (IsoMet 4000, Buehler, USA), mounted in epoxy resin, and sequentially ground using silicon carbide abrasive papers with grit sizes ranging from 320 to 2000. The specimens were subsequently polished using diamond suspensions on an automatic grinding and polishing system (EcoMet 300 Pro, Buehler, USA) to obtain mirror-like surfaces. The polished samples were chemically etched with Keller's reagent to reveal the microstructure. Optical observations were performed using a metallurgical optical microscope (BX53M, Olympus Corporation, Japan) operated within a magnification range of 50×–1000× to investigate grain morphology, the distribution of eutectic silicon particles, and the presence of intermetallic phases. Higher-resolution examinations of phase morphology, fracture characteristics, and elemental distribution were conducted using a field-emission scanning electron microscope (JSM-7610F Plus, JEOL Ltd., Japan) operating at an accelerating voltage of 0.1–30 kV and equipped with an energy-dispersive X-ray spectroscopy detector (X-MaxN 50, Oxford Instruments, United Kingdom) capable of elemental detection from boron (B) to uranium (U) with an energy resolution of 127 eV.

The phase composition and crystallographic characteristics of the investigated alloys were analyzed using a powder X-ray diffractometer (X'Pert PRO MPD, Malvern Panalytical, Netherlands) employing Cu Kα radiation with a wavelength of $\lambda = 1.5406$ Å. Diffraction patterns were collected over a 2θ range of 20°–80° using a step size of 0.02° to identify the constituent phases and evaluate the structural modifications induced by the different heat-treatment conditions.

Mechanical characterization was carried out in accordance with relevant ASTM standards. The hardness of each specimen was measured using a digital Vickers hardness tester (HMV-G21, Shimadzu Corporation, Japan) under a load of 10 kgf (HV10) with a dwell time of 15 s. A minimum of five indentations was performed at different locations on each specimen, and the average hardness value was reported to ensure measurement reliability and minimize local microstructural effects.

Tensile testing was conducted using an electromechanical universal testing machine (Instron 5982, Instron Corporation, USA) with a maximum load capacity of 100 kN, following the ASTM E8/E8M standard. Standard dog-bone specimens were tested at room temperature using a constant crosshead speed of 2 mm min^{-1}. The ultimate tensile strength (UTS), yield strength (YS), and percentage elongation (%El) were determined from the engineering stress–strain curves generated during testing.

*Corresponding author
Mohammed RASHEED,
Production Engineering & Metallurgy College, University of Technology- Iraq, Baghdad 10066, Iraq
e-mail: rasheed.mohammed40@yahoo.com

Impact toughness was evaluated using a pendulum-type Charpy impact testing machine (JBW-300B, Time Group Inc., China) with a maximum energy capacity of 300 J in accordance with ASTM E23. Standard V-notched specimens were employed to determine the energy absorption capability of the alloys under sudden loading conditions, and the absorbed impact energy values were compared among the different thermal processing states.

The wear behavior of the specimens was investigated using a pin-on-disc tribometer (TR-20LE, Ducom Instruments, India) following ASTM G99 under dry sliding conditions. The experiments were performed using a constant normal load, sliding speed, and sliding distance. The tribometer operates within a load range of 1–200 N and rotational speeds of 50–2000 rpm. Prior to and after wear testing, the specimens were weighed using a precision analytical balance (AS 220.R2, RADWAG, Poland) with a readability of 0.1 mg. The wear rate was subsequently calculated from the measured mass loss values.

Fatigue performance was assessed using an RR Moore-type rotating bending fatigue testing machine (GUNT Hamburg, Germany) in accordance with ASTM E466. The machine operates at frequencies ranging from 20 to 50 Hz and permits the application of stress amplitudes up to 1000 MPa. Fatigue life was determined by recording the number of cycles to failure at selected stress amplitudes, and S–N curves were constructed to compare the endurance behavior of the investigated heat-treatment conditions.

Finally, the fracture surfaces of specimens subjected to tensile and fatigue testing were examined using the JEOL JSM-7610F Plus field-emission scanning electron microscope to identify the dominant failure mechanisms and to assess the influence of thermal processing on crack initiation and propagation behavior. The integration of microstructural characterization techniques with comprehensive mechanical testing provided a detailed understanding of the role of heat treatment in enhancing the performance, durability, and reliability of aluminum piston alloys intended for demanding automotive piston applications. Fig. 1 presents the overall experimental workflow adopted in this study for evaluating the mechanical improvement of aluminum piston alloys under different thermal processing conditions. The figure illustrates the sequence of procedures beginning with the preparation of the aluminum piston alloy and the fabrication of four representative samples, namely the as-cast alloy (S1), solution-treated alloy (S2), T6-treated alloy (S3), and over-aged alloy (S4). The prepared specimens were machined according to the required dimensions for characterization and mechanical testing. Microstructural characterization was subsequently performed using optical microscopy (OM), scanning electron microscopy coupled with energy-dispersive X-ray spectroscopy (SEM/EDS), and X-ray diffraction (XRD) to investigate grain morphology, elemental distribution, fracture features, and phase composition. Mechanical performance was evaluated using standardized ASTM procedures, including Vickers hardness testing (ASTM E92), tensile testing (ASTM E8/E8M), Charpy impact testing (ASTM E23), pin-on-disc wear testing (ASTM G99), and rotating bending fatigue testing (ASTM E466). Finally, the experimental data obtained from these analyses were correlated to establish the relationship between thermal processing, microstructural evolution, and mechanical behavior, thereby enabling the identification of the optimum heat-treatment condition for automotive piston applications.

*Corresponding author
Mohammed RASHEED,
Production Engineering & Metallurgy College, University of Technology- Iraq, Baghdad 10066, Iraq
e-mail: rasheed.mohammed40@yahoo.com

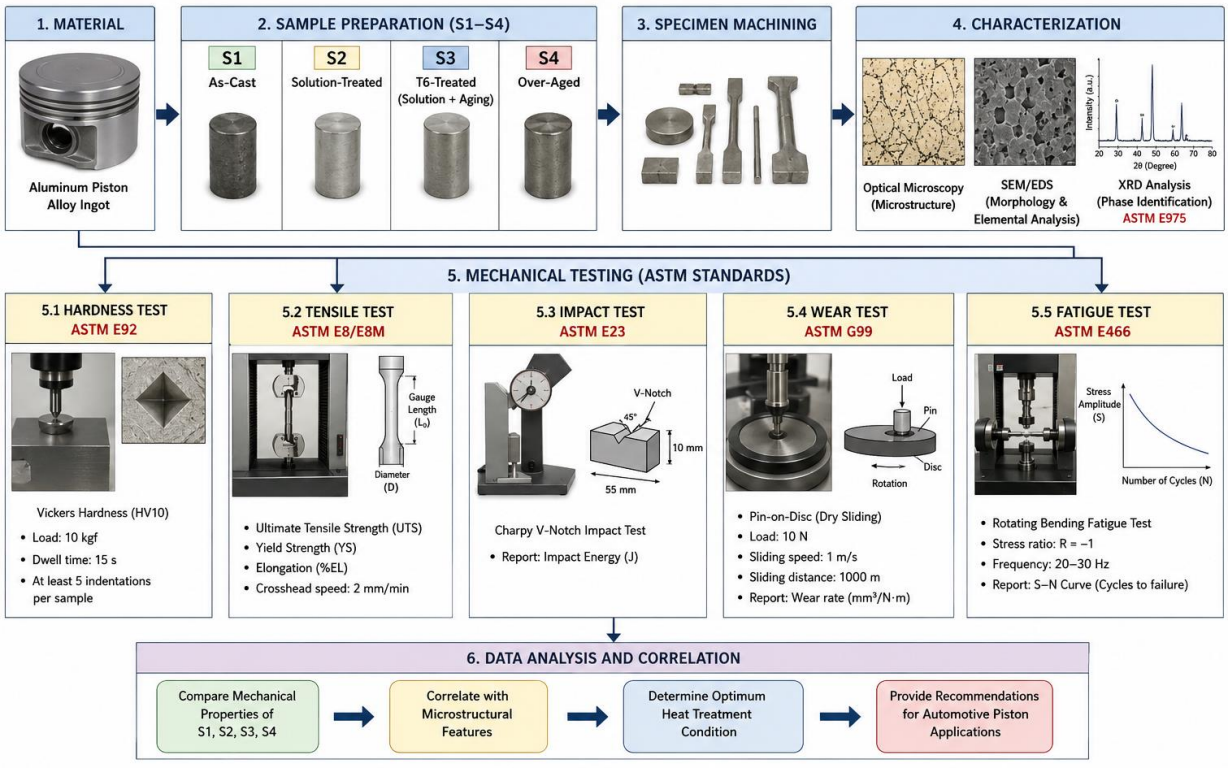

Fig. 1. Schematic representation of the experimental methodology and ASTM-standardized characterization procedures employed for the investigation of aluminum piston alloys under different heat-treatment conditions. The workflow includes sample preparation of S1 (as-cast), S2 (solution-treated), S3 (T6-treated), and S4 (over-aged) alloys, followed by specimen machining, microstructural characterization using OM, SEM/EDS, and XRD, and mechanical evaluation through hardness (ASTM E92), tensile (ASTM E8/E8M), impact (ASTM E23), wear (ASTM G99), and fatigue (ASTM E466) testing to determine the relationship between thermal processing and mechanical performance.

RESULTS AND DISCUSSION

MICROSTRUCTURAL ANALYSIS (OM/SEM/EDS)

Fig. 2 presents the microstructural evolution of the aluminum piston alloys subjected to different heat-treatment conditions through (a) optical microscopy (OM), (b) scanning electron microscopy (SEM), and (c) energy-dispersive X-ray spectroscopy (EDS) analyses. The combined characterization techniques provide valuable information regarding the morphology of the α-Al matrix, the distribution and morphology of eutectic silicon particles, the behavior of intermetallic phases, and the corresponding elemental composition associated with the observed microstructural changes. The optical micrograph of the as-cast alloy (S1) (Fig. 2(a)) reveals a typical hypoeutectic Al–Si piston alloy microstructure consisting of coarse α-Al dendrites surrounded by an interconnected eutectic network containing irregular silicon particles and intermetallic compounds. The eutectic Si particles exhibit angular and acicular morphologies with non-uniform distribution throughout the matrix. In addition, relatively large intermetallic constituents are observed along interdendritic regions, indicating segregation during solidification. Such coarse and heterogeneous features are generally considered detrimental to mechanical performance because they act as preferential sites for stress concentration and crack initiation under external loading [9].

Following solution treatment (S2), a noticeable refinement and homogenization of the microstructure are observed. The optical images indicate partial dissolution of coarse intermetallic phases and fragmentation of eutectic silicon particles. Compared with S1, the α-Al matrix appears more uniform, while the Si particles become smaller and more rounded. The reduction in microstructural heterogeneity can be attributed to enhanced diffusion during solution treatment, which promotes elemental redistribution and decreases

*Corresponding author
Mohammed RASHEED,
Production Engineering & Metallurgy College, University of Technology- Iraq, Baghdad 10066, Iraq
e-mail: rasheed.mohammed40@yahoo.com

localized compositional gradients. This microstructural modification is expected to improve ductility and reduce the susceptibility to premature crack formation.

The T6-treated sample (S3) exhibits the most refined and homogeneous microstructure among all investigated conditions. The OM images reveal a uniform distribution of fine silicon particles embedded within the aluminum matrix. The eutectic constituents appear spheroidized, and the overall microstructure is characterized by a dense dispersion of small precipitates resulting from artificial aging. The refinement of silicon particles and the formation of finely distributed strengthening precipitates effectively impede dislocation movement and inhibit crack propagation. Consequently, the S3 condition is anticipated to exhibit the highest hardness, tensile strength, wear resistance, and fatigue performance [10].

In contrast, the over-aged specimen (S4) demonstrates a deterioration of the refined microstructure developed during T6 treatment. The optical micrographs show coarsening of silicon particles and the growth of precipitates within the matrix. Although the microstructure remains more homogeneous than that of the as-cast alloy, the enlarged precipitates and coarse eutectic particles reduce the effectiveness of precipitation strengthening. The coarsened microstructural constituents may facilitate localized plastic deformation and contribute to reductions in strength and fatigue resistance compared with the T6-treated condition.

The SEM micrographs presented in Fig. 2(b) provide higher-resolution observations of the morphological changes induced by thermal processing. The as-cast sample (S1) exhibits large eutectic silicon plates and elongated intermetallic phases distributed around the α-Al dendrites. These sharp-edged particles serve as stress raisers and may promote brittle fracture under cyclic loading. In S2, the silicon particles become less angular and more fragmented, confirming the beneficial effect of solution treatment on reducing particle size and improving phase distribution. The T6-treated alloy (S3) displays the most favorable morphology, characterized by finely dispersed and nearly spheroidized particles uniformly distributed throughout the matrix. Such a microstructure minimizes stress concentration and enhances load transfer efficiency between the matrix and secondary phases. Conversely, S4 shows evidence of precipitate coarsening and particle agglomeration, indicating the onset of over-aging. The larger particles observed in this condition decrease the obstruction to dislocation motion and compromise the strengthening effect achieved in S3.

The EDS spectra shown in Fig. 2(c) further confirm the elemental constitution of the observed phases. In all samples, aluminum and silicon represent the dominant elements, reflecting the Al–Si nature of the piston alloy. Minor amounts of Cu, Mg, and Fe are also detected, corresponding to the alloying additions and intermetallic constituents commonly present in commercial piston alloys. The EDS analysis of S1 indicates localized enrichment of Si and Fe within coarse eutectic and intermetallic regions. Following solution treatment (S2), a more homogeneous elemental distribution is observed due to the dissolution of segregated phases. The T6-treated sample (S3) exhibits the most uniform elemental distribution, suggesting efficient diffusion and precipitation processes during artificial aging. In contrast, S4 demonstrates slight elemental segregation associated with precipitate growth and coarsening during prolonged aging.

A comparative assessment of the four conditions clearly demonstrates that thermal processing has a profound influence on the microstructural characteristics of aluminum piston alloys. The as-cast condition exhibits the coarsest and most heterogeneous microstructure, which is generally associated with inferior mechanical performance. Solution treatment improves structural homogeneity through phase dissolution and silicon refinement. The T6 treatment provides the optimum microstructure by producing uniformly distributed fine precipitates and spheroidized silicon particles, thereby maximizing the strengthening effect. Over-aging, however, reduces the effectiveness of precipitation hardening due to precipitate coarsening and particle growth. Therefore, based on the OM, SEM, and EDS observations, the T6-treated alloy (S3) is expected to exhibit the most favorable combination of hardness, strength, wear resistance, and fatigue durability among the investigated samples [11].

*Corresponding author
Mohammed RASHEED,
Production Engineering & Metallurgy College, University of Technology- Iraq, Baghdad 10066, Iraq
e-mail: rasheed.mohammed40@yahoo.com

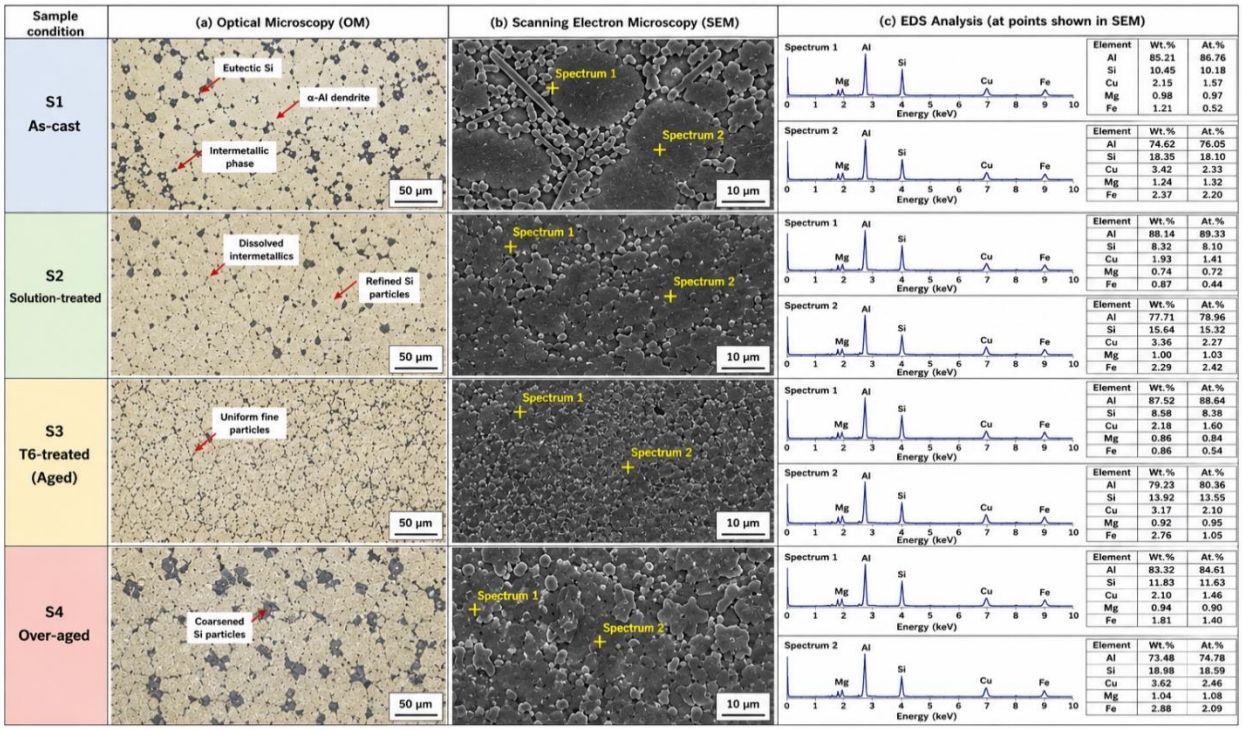

Fig. 2. Microstructural characterization of aluminum piston alloys under different heat-treatment conditions: (a) optical microscopy (OM) images showing the evolution of α-Al dendrites, eutectic silicon particles, and intermetallic phases; (b) SEM micrographs illustrating the morphological changes and distribution of secondary phases; and (c) EDS spectra and elemental compositions of representative regions for S1 (as-cast), S2 (solution-treated), S3 (T6-treated), and S4 (over-aged) samples.

XRD ANALYSIS

Fig. 3 presents the X-ray diffraction patterns of the aluminum piston alloys subjected to different thermal processing conditions, namely S1 (as-cast), S2 (solution-treated), S3 (T6-treated), and S4 (over-aged). The XRD analysis confirmed that all investigated samples mainly consisted of an aluminum-rich matrix accompanied by eutectic silicon and minor intermetallic phases. The dominant phase identified in all diffraction patterns was the α-Al phase, indexed according to JCPDS/PDF card No. 04-0787. This phase possesses a face-centered cubic (FCC) crystal structure with a lattice parameter of approximately a = 4.049 Å, belonging to the Fm-3m space group and the cubic crystal system [12]. The principal α-Al diffraction peaks appeared at approximately 38.47°, 44.74°, 65.13°, and 78.22°, corresponding to the (111), (200), (220), and (222) crystallographic planes, respectively. Because α-Al exhibits cubic symmetry, the crystallographic angles satisfy the relationship α = β = γ = 90°. In addition to the aluminum matrix, silicon reflections were observed in all samples and indexed according to JCPDS/PDF card No. 27-1402. Silicon crystallizes in a diamond cubic structure with a lattice parameter of approximately a = 5.431 Å and belongs to the Fd-3m space group. The characteristic Si diffraction peaks were detected at approximately 28.44°, 47.30°, 56.12°, and 69.13°, corresponding to the (111), (220), (311), and (400) planes, respectively. The presence of these silicon peaks confirms the existence of eutectic Si particles distributed within the aluminum matrix, which play an important role in controlling hardness, wear resistance, and thermal stability. Similar to α-Al, silicon possesses cubic symmetry with crystallographic angles of α = β = γ = 90° [13-15].

Minor diffraction peaks associated with the strengthening phase Al_2Cu were detected, particularly in the heat-treated specimens. This phase was indexed using JCPDS/PDF card No. 33-0248 and exhibited a tetragonal crystal structure with lattice parameters of approximately a = 6.067 Å and c = 4.877 Å. The corresponding space group is I4/mcm. The major Al_2Cu reflections appeared near 47.1°, 64.0°, and 74.3°, corresponding to the (200), (220), and (311) planes, respectively. The appearance and increased intensity of

*Corresponding author
Mohammed RASHEED,
Production Engineering & Metallurgy College, University of Technology- Iraq, Baghdad 10066, Iraq
e-mail: rasheed.mohammed40@yahoo.com

these peaks in the T6-treated alloy indicate the formation of fine strengthening precipitates during artificial aging. For this tetragonal phase, the crystallographic angles remain $\alpha = \beta = \gamma = 90°$. A weak Fe-containing intermetallic phase identified as Al5FeSi was also detected. This phase was indexed according to JCPDS/PDF card No. 34-0492 and generally exhibits a monoclinic crystal structure with approximate lattice parameters of $a \approx 6.12$ Å, $b \approx 6.25$ Å, and $c \approx 4.15$ Å, belonging to the C2/m space group. The corresponding diffraction peaks appeared at approximately 39.1°, 59.2°, and 69.5°. Because of its monoclinic symmetry, the crystallographic angles satisfy $\alpha = \gamma = 90°$, whereas $\beta \neq 90°$. The occurrence of this phase is commonly attributed to Fe impurities or alloying additions present in commercial aluminum piston alloys [16-18].

The XRD patterns further revealed that heat treatment did not introduce any major new crystalline phases but significantly modified the relative peak intensities and peak broadening of the existing phases. The as-cast sample (S1) exhibited relatively broad diffraction peaks, indicating a higher concentration of lattice defects and residual stresses inherited from the casting process. Following solution treatment (S2), the diffraction peaks became sharper, suggesting improved structural homogeneity and partial stress relief. The most pronounced improvement was observed in the T6-treated alloy (S3), which displayed the sharpest and most intense α-Al and secondary-phase reflections, reflecting enhanced crystallinity and effective precipitation strengthening. In contrast, the over-aged sample (S4) showed slight peak broadening and moderate reductions in peak intensity relative to S3, indicating precipitate coarsening and the gradual deterioration of the strengthening effect [19].

The structural parameters obtained from Table 1 provide quantitative evidence of these changes. The interplanar spacing values were determined using Bragg's law, $n\lambda = 2d\sin\theta$, where n is the diffraction order, λ is the wavelength of the Cu Kα radiation (1.5406 Å), d is the interplanar spacing, and θ is the Bragg angle, while the crystallite sizes were estimated using the Debye–Scherrer equation, $D_{cs} = K\lambda/\beta\cos\theta$, where K is the shape factor (0.9), λ is the X-ray wavelength, β is the full width at half maximum (FWHM) in radians, and θ is the Bragg angle. The average crystallite size increased progressively from 28.05 nm in the as-cast alloy (S1) to 31.00 nm after solution treatment (S2), reaching a maximum value of 37.27 nm for the T6-treated sample (S3). This represents an increase of approximately 32.9% relative to S1. For example, the crystallite size associated with the α-Al (111) reflection increased from 28.05 nm in S1 to 31.16 nm in S2 and further to 38.25 nm in S3, before decreasing to 32.36 nm in the over-aged sample (S4). Similarly, the Si (111) reflection increased from 29.27 nm in S1 to 32.78 nm in S2 and reached 39.03 nm in S3, followed by a reduction to 34.15 nm in S4. These findings indicate that the T6 treatment effectively promoted crystallite growth and improved crystal perfection, whereas over-aging partially diminished this beneficial effect [20].

The defect-related parameters summarized in Table 2 further support this interpretation. The lattice microstrain values were calculated using $\varepsilon = \beta/4\tan\theta$, where β represents the peak broadening and θ is the diffraction angle; whereas the dislocation density was estimated from $\delta = 1/D_{cs}^2$. The as-cast sample exhibited the highest microstrain values, ranging from 2.63×10^{-3} to 4.89×10^{-3}, indicating severe lattice distortion and internal residual stresses. After solution treatment, the microstrain decreased to 2.37×10^{-3} – 4.48×10^{-3}, while the T6-treated alloy exhibited the lowest values, ranging from 1.93×10^{-3} to 3.81×10^{-3}. The over-aged condition showed slightly higher values (2.28×10^{-3}–4.35×10^{-3}), suggesting the reappearance of local lattice distortions due to precipitate coarsening. A similar trend was observed for the dislocation density values. The as-cast alloy exhibited the highest defect concentration, ranging from 1.17×10^{-3} to 1.39×10^{-3} nm^{-2}, whereas S2 showed reduced values of 0.93×10^{-3}–1.14×10^{-3} nm^{-2}. The T6-treated alloy displayed the lowest dislocation density values, ranging from only 0.66×10^{-3} to 0.78×10^{-3} nm^{-2}, corresponding to reductions of approximately 43–48% relative to S1. In contrast, the over-aged sample exhibited intermediate values between 0.86×10^{-3} and 1.06×10^{-3} nm^{-2}, reflecting a decline in crystal perfection after prolonged aging. The preferred crystallographic orientation was evaluated using the texture coefficient equation, $TC(hkl) = \frac{\frac{I(hkl)}{I_o(hkl)}}{\frac{1}{N}\sum_{i=1}^{N}\frac{I(hkl)}{I_o(hkl)}}$, where I(hkl) is the measured intensity of a given diffraction plane, $I_o(hkl)$ is the standard intensity obtained from the reference PDF database, and N is the number of reflections considered. The as-cast alloy exhibited nearly random orientation, with TC values ranging from 0.90 to 1.03. Solution treatment increased the texture coefficient to 0.97–1.08, whereas the T6-treated sample exhibited the strongest preferred orientation, with values ranging from 1.10 to 1.21. The highest

*Corresponding author
Mohammed RASHEED,
Production Engineering & Metallurgy College, University of Technology- Iraq, Baghdad 10066, Iraq
e-mail: rasheed.mohammed40@yahoo.com

texture coefficients were recorded for the Si (220) plane (1.21) and the α-Al (200) plane (1.19). The over-aged alloy retained moderate texture characteristics, with TC values between 1.01 and 1.12, although these values were lower than those observed for S3 [21].

Finally, the unit-cell volumes listed in Table 2 were calculated using $V = a^3$ for the cubic α-Al and Si phases. The α-Al phase exhibited unit-cell volumes ranging from 66.29 to 66.39 Å^3, whereas the Si phase remained nearly constant between 160.15 and 160.24 Å^3. These negligible variations indicate that heat treatment primarily affected the defect structure and crystallographic quality rather than altering the intrinsic crystal lattice dimensions. Therefore, the combined interpretation of Fig. 3, Table 1, and Table 2 confirms that the T6-treated alloy (S3) possessed the most favorable crystallographic characteristics, characterized by the largest crystallite size, lowest lattice strain, reduced dislocation density, and strongest preferred orientation. These structural improvements provide a clear explanation for the superior mechanical performance expected for the T6-treated aluminum piston alloy.

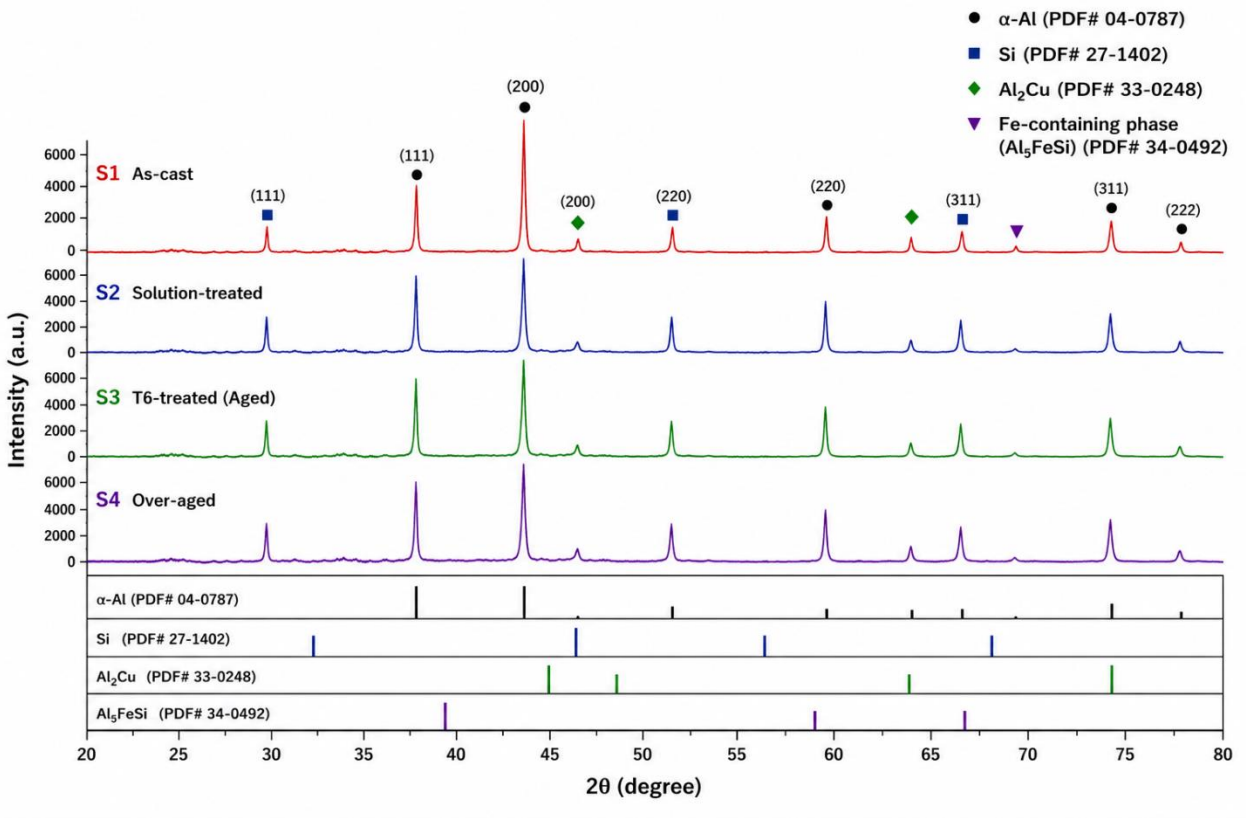

Fig. 3. XRD patterns of aluminum piston alloys subjected to different heat-treatment conditions: S1 (as-cast), S2 (solution-treated), S3 (T6-treated), and S4 (over-aged)

*Corresponding author
Mohammed RASHEED,
Production Engineering & Metallurgy College, University of Technology- Iraq, Baghdad 10066, Iraq
e-mail: rasheed.mohammed40@yahoo.com

Table 1. XRD structural parameters of aluminum piston alloys under different heat-treatment conditions, including diffraction angle (2θ), full width at half maximum (FWHM), crystallographic planes (hkl), interplanar spacing (d-spacing), crystallite size (D_{cs}), and average crystallite size ($D_{cs\text{-}ave}$) calculated from the major diffraction peaks using the Debye–Scherrer method.

Samples	2θ (°)	FWHM (°)	(hkl)	d-Spacing (Å)	Dcs (nm)	Dcs-ave (nm)
S1	28.44	0.28	Si (111)	3.136	29.27	28.05
S1	38.47	0.30	α-Al (111)	2.338	28.05	
S1	44.74	0.32	α-Al (200)	2.024	26.85	
S1	47.30	0.31	Si (220)	1.920	27.98	
S1	65.13	0.34	α-Al (220)	1.431	27.72	
S1	78.22	0.36	α-Al (222)	1.221	28.44	
S2	28.44	0.25	Si (111)	3.136	32.78	31.00
S2	38.47	0.27	α-Al (111)	2.338	31.16	
S2	44.74	0.29	α-Al (200)	2.024	29.62	
S2	47.30	0.28	Si (220)	1.920	30.97	
S2	65.13	0.31	α-Al (220)	1.431	30.41	
S2	78.22	0.33	α-Al (222)	1.221	31.03	
S3	28.44	0.21	Si (111)	3.136	39.03	37.27
S3	38.47	0.22	α-Al (111)	2.338	38.25	
S3	44.74	0.24	α-Al (200)	2.024	35.80	
S3	47.30	0.23	Si (220)	1.920	37.71	
S3	65.13	0.26	α-Al (220)	1.431	36.26	
S3	78.22	0.28	α-Al (222)	1.221	36.57	
S4	28.44	0.24	Si (111)	3.136	34.15	32.12
S4	38.47	0.26	α-Al (111)	2.338	32.36	
S4	44.74	0.28	α-Al (200)	2.024	30.68	
S4	47.30	0.27	Si (220)	1.920	32.12	
S4	65.13	0.30	α-Al (220)	1.431	31.42	
S4	78.22	0.32	α-Al (222)	1.221	32.00	

Table 2. Lattice parameters, microstrain, dislocation density, texture coefficient, and unit-cell volume of aluminum piston alloys calculated from the individual diffraction peaks.

Sample	2θ (°)	(hkl)	a (Å)	c (Å)	Microstrain, ε ($\times10^{-3}$)	Dislocation Density, δ ($\times10^{-3}$ nm^{-2})	Texture Coefficient, TC	Unit-Cell Volume, V (Å^3)
S1	28.44	Si (111)	5.432	5.432	2.79	1.17	0.92	160.24
S1	38.47	α-Al (111)	4.049	4.049	2.63	1.27	0.96	66.39
S1	44.74	α-Al (200)	4.048	4.048	2.86	1.39	1.01	66.34
S1	47.30	Si (220)	5.431	5.431	2.95	1.28	1.03	160.15
S1	65.13	α-Al (220)	4.048	4.048	3.47	1.30	0.94	66.34
S1	78.22	α-Al (222)	4.049	4.049	4.89	1.24	0.90	66.39
S2	28.44	Si (111)	5.432	5.432	2.49	0.93	0.97	160.24
S2	38.47	α-Al (111)	4.049	4.049	2.37	1.03	1.02	66.39
S2	44.74	α-Al (200)	4.048	4.048	2.59	1.14	1.05	66.34
S2	47.30	Si (220)	5.431	5.431	2.67	1.04	1.08	160.15
S2	65.13	α-Al (220)	4.048	4.048	3.16	1.08	0.99	66.34
S2	78.22	α-Al (222)	4.049	4.049	4.48	1.04	0.98	66.39
S3	28.44	Si (111)	5.432	5.432	2.09	0.66	1.11	160.24
S3	38.47	α-Al (111)	4.047	4.047	1.93	0.68	1.15	66.29
S3	44.74	α-Al (200)	4.047	4.047	2.14	0.78	1.19	66.29
S3	47.30	Si (220)	5.431	5.431	2.19	0.70	1.21	160.15
S3	65.13	α-Al (220)	4.047	4.047	2.65	0.76	1.14	66.29
S3	78.22	α-Al (222)	4.048	4.048	3.81	0.75	1.10	66.34
S4	28.44	Si (111)	5.432	5.432	2.39	0.86	1.04	160.24
S4	38.47	α-Al (111)	4.048	4.048	2.28	0.96	1.07	66.34
S4	44.74	α-Al (200)	4.048	4.048	2.50	1.06	1.10	66.34

*Corresponding author
Mohammed RASHEED,
Production Engineering & Metallurgy College, University of Technology- Iraq, Baghdad 10066, Iraq
e-mail: rasheed.mohammed40@yahoo.com

S4	47.30	Si (220)	5.431	5.431	2.57	0.97	1.12	160.15
S4	65.13	α-Al (220)	4.048	4.048	3.05	1.01	1.05	66.34
S4	78.22	α-Al (222)	4.049	4.049	4.35	0.98	1.01	66.39

HARDNESS MEASUREMENTS

Fig. 4 presents the Vickers hardness values of the aluminum piston alloy samples subjected to different heat-treatment conditions, namely S1 (as-cast), S2 (solution-treated), S3 (T6-treated), and S4 (over-aged). The figure shows that the hardness increased progressively from the as-cast condition to the T6-treated condition, indicating the beneficial influence of thermal processing on strengthening the aluminum matrix. The as-cast sample exhibited the lowest hardness due to its coarse dendritic structure, non-uniform eutectic Si distribution, and higher defect concentration. After solution treatment, the hardness improved slightly as a result of partial dissolution of soluble phases, homogenization of the matrix, and refinement of eutectic silicon particles. The highest hardness was observed for the T6-treated sample, which can be attributed to the formation of fine and uniformly distributed strengthening precipitates, improved crystallinity, and reduced dislocation density. However, the over-aged sample showed a decrease in hardness compared with S3 because prolonged aging promoted precipitate coarsening and reduced the effectiveness of precipitation strengthening. Therefore, the hardness trend confirms that the T6-treated condition provides the most effective strengthening response among the investigated aluminum piston alloy samples [22].

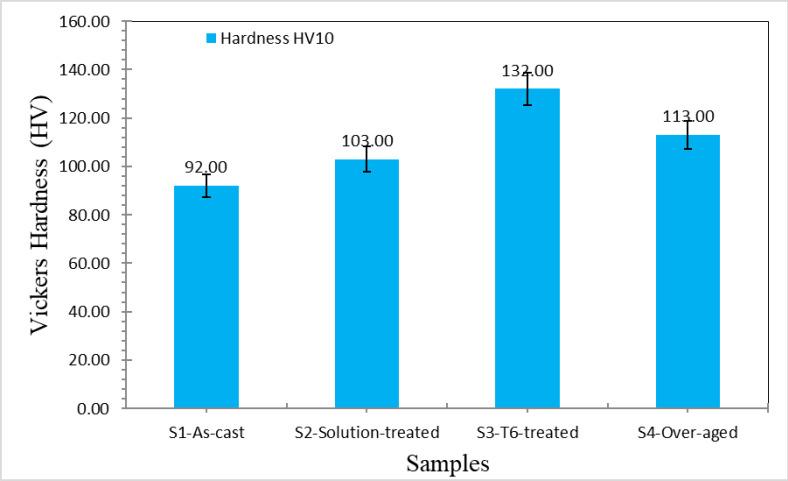

Fig. 4. Vickers hardness variation of aluminum piston alloys under different heat-treatment conditions: S1 (as-cast), S2 (solution-treated), S3 (T6-treated), and S4 (over-aged).

TENSILE PROPERTIES

Fig. 5 presents the tensile behavior of the aluminum piston alloys subjected to different heat-treatment conditions, including (a) ultimate tensile strength (UTS), (b) yield strength (YS), (c) percentage elongation (%El), and (d) engineering stress–strain curves for S1 (as-cast), S2 (solution-treated), S3 (T6-treated), and S4 (over-aged) samples. The results clearly demonstrate that thermal processing had a significant influence on the tensile performance of the investigated alloys, and the observed trends are in good agreement with the microstructural and crystallographic modifications discussed in the previous sections.

The as-cast alloy (S1) exhibited the lowest tensile performance among all investigated samples, with a yield strength of 128 MPa, an ultimate tensile strength of 185 MPa, and an elongation of 4.8%. The relatively poor tensile properties can be attributed to the coarse dendritic α-Al matrix, non-uniform distribution of eutectic silicon particles, and the presence of casting defects and residual stresses. The coarse acicular silicon particles act as stress concentration sites that facilitate crack initiation and propagation, thereby limiting both the load-bearing capacity and ductility of the alloy.

Following solution treatment, the tensile properties improved noticeably. The S2 sample exhibited a yield strength of 145 MPa, an ultimate tensile strength of 210 MPa, and an elongation of 6.2%. Compared with

*Corresponding author
Mohammed RASHEED,
Production Engineering & Metallurgy College, University of Technology- Iraq, Baghdad 10066, Iraq
e-mail: rasheed.mohammed40@yahoo.com

the as-cast condition, the yield strength increased by approximately 13.3%, while the ultimate tensile strength improved by 13.5%. Moreover, the elongation increased by approximately 29.2%, indicating enhanced ductility. These improvements can be attributed to the dissolution of soluble phases, homogenization of the matrix, and refinement of eutectic silicon particles during solution treatment, which reduced stress concentration effects and promoted more uniform plastic deformation.

The most remarkable enhancement in tensile performance was observed for the T6-treated alloy (S3). This sample exhibited the highest yield strength of 182 MPa, ultimate tensile strength of 265 MPa, and elongation of 7.1%. Relative to S1, the yield strength increased by approximately 42.2%, while the ultimate tensile strength improved by 43.2%. The elongation also increased by approximately 47.9%, indicating that the T6 treatment simultaneously improved both strength and ductility. Compared with the solution-treated sample, S3 showed additional improvements of 25.5% in yield strength, 26.2% in ultimate tensile strength, and 14.5% in elongation. These superior tensile properties are primarily attributed to precipitation hardening resulting from the formation of fine and uniformly distributed Al_2Cu precipitates during artificial aging. Furthermore, the refined eutectic silicon morphology, increased crystallite size, reduced microstrain, and lower dislocation density observed in the XRD analysis contributed significantly to the enhanced tensile response.

In contrast, the over-aged sample (S4) exhibited a decline in tensile performance compared with the T6-treated condition. The measured yield strength, ultimate tensile strength, and elongation were 158 MPa, 232 MPa, and 5.9%, respectively. Although these values remained higher than those of the as-cast alloy, they were lower than those obtained for S3. Specifically, compared with the T6-treated sample, the yield strength decreased by approximately 13.2%, the ultimate tensile strength decreased by 12.5%, and the elongation decreased by 16.9%. The deterioration in tensile performance can be explained by precipitate coarsening during prolonged aging, which reduces the effectiveness of precipitation strengthening and facilitates localized deformation. The trend is: S3 > S4 > S2 > S1 for tensile strength. The engineering stress–strain curves shown in Fig. 5(d) further illustrate the influence of thermal processing on the deformation behavior of the alloys. The as-cast sample exhibited the lowest flow stress and fractured at relatively low strain values, indicating limited plastic deformation. The solution-treated alloy displayed improved strain hardening capability and higher fracture strain. The T6-treated sample exhibited the highest stress levels throughout the deformation process and sustained larger strains prior to fracture, demonstrating an excellent combination of strength and ductility. Conversely, the over-aged alloy maintained intermediate behavior between S2 and S3, reflecting the partial loss of strengthening associated with precipitate growth.

The tensile results indicate that the mechanical performance of aluminum piston alloys can be substantially improved through appropriate heat treatment. The T6-treated condition provided the optimum balance between strength and ductility, while the as-cast condition exhibited the poorest tensile behavior. The over-aged condition retained moderate tensile properties but failed to achieve the strengthening efficiency observed in the T6-treated alloy. These findings are consistent with the microstructural observations, hardness measurements, and XRD analyses, confirming that the enhanced tensile performance of the T6-treated sample originates from microstructural refinement, precipitation strengthening, and improved crystallographic quality [23].

*Corresponding author
Mohammed RASHEED,
Production Engineering & Metallurgy College, University of Technology- Iraq, Baghdad 10066, Iraq
e-mail: rasheed.mohammed40@yahoo.com

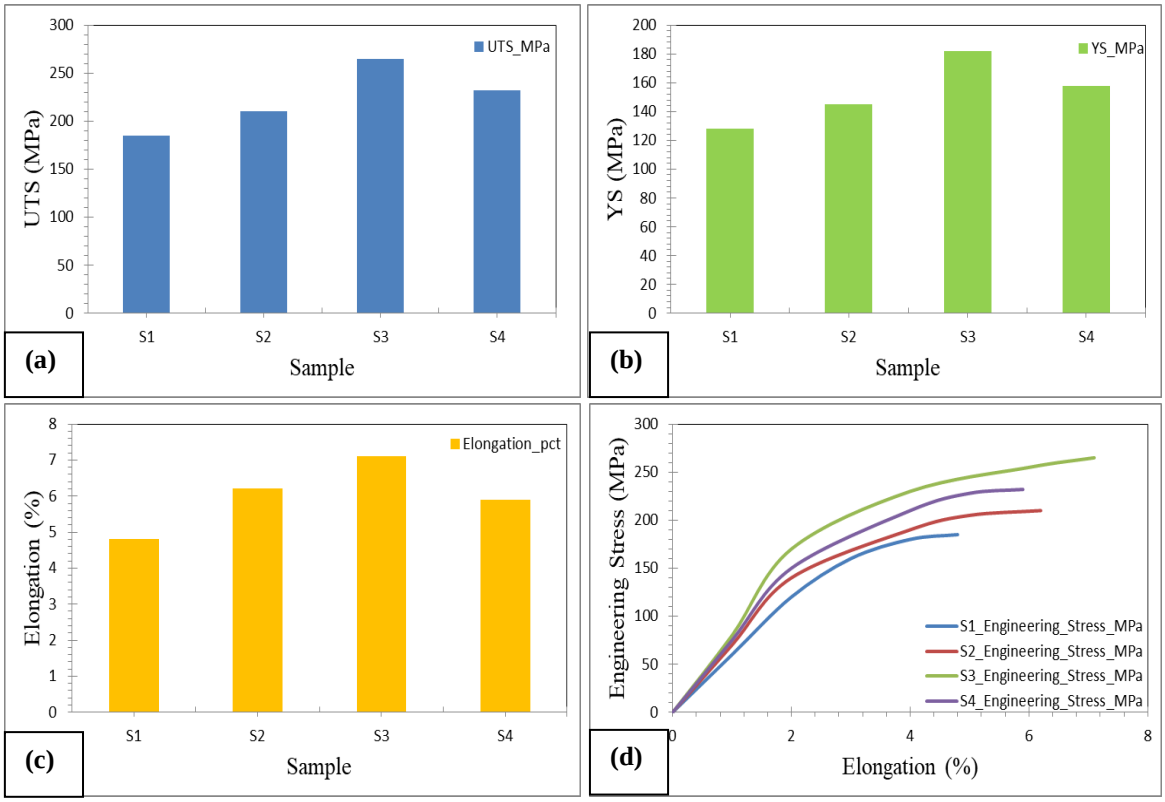

Fig. 5. Tensile properties of aluminum piston alloys under different heat-treatment conditions: (a) ultimate tensile strength (UTS), (b) yield strength (YS), (c) percentage elongation (%El), and (d) engineering stress–strain curves of S1 (as-cast), S2 (solution-treated), S3 (T6-treated), and S4 (over-aged) samples, illustrating the influence of thermal processing on strength, ductility, and deformation behavior. The T6-treated alloy exhibited the optimum tensile performance due to precipitation hardening and microstructural refinement, whereas the over-aged condition showed a reduction in tensile properties because of precipitate coarsening.

WEAR BEHAVIOR

Table 3 presents the tribological parameters of the aluminum piston alloys subjected to different heat-treatment conditions, including mass loss, wear rate, and coefficient of friction (COF). The wear rate values were determined using the relation [24]:

$$\text{Wear rate} = \frac{\Delta m}{(\rho \times L)} \quad (1)$$

where Δm is the mass loss (g), ρ is the density of the alloy (g·cm-3), and L is the sliding distance (m). According to Eq. 1, a lower mass loss corresponds directly to a lower wear rate and, consequently, improved wear resistance. The results listed in Table 3 clearly demonstrate that thermal processing significantly influenced the tribological behavior of the investigated alloys.

The as-cast alloy (S1) exhibited the highest mass loss (18.6 mg), the highest wear rate (4.85 × 10-4 mm3/N·m), and the largest coefficient of friction (0.62), indicating the poorest resistance to material removal during sliding. Based on Eq. 1, the large value of Δm recorded for S1 resulted in the highest wear rate among all samples. This inferior tribological performance can be attributed to the coarse eutectic silicon morphology, heterogeneous microstructure, and relatively low hardness of the as-cast alloy, which promote severe plastic deformation, crack initiation, and delamination during wear. The high COF further suggests unstable sliding conditions and increased frictional losses at the contact interface.

After solution treatment, the wear performance improved considerably. The S2 sample exhibited a mass loss of 14.2 mg, a wear rate of 3.72 × 10-4 mm3/N·m, and a coefficient of friction of 0.56. According to Eq. 1, the reduction in mass loss resulted in a proportional decrease in wear rate. Compared with S1, the mass loss decreased by approximately 23.7%, while the wear rate and COF were reduced by 23.3% and 9.7%, respectively. These improvements can be attributed to the dissolution of soluble phases and enhanced

*Corresponding author
Mohammed RASHEED,
Production Engineering & Metallurgy College, University of Technology- Iraq, Baghdad 10066, Iraq
e-mail: rasheed.mohammed40@yahoo.com

microstructural homogeneity, which reduce stress concentration sites and improve the load-bearing capability of the alloy surface during sliding contact.

The most remarkable enhancement in tribological performance was observed for the T6-treated alloy (S3). This sample exhibited the lowest mass loss (8.9 mg), the smallest wear rate (2.15 × 10-4 mm3/N·m), and the lowest coefficient of friction (0.48). As predicted by Eq. 1, the substantial reduction in Δm directly contributed to the lowest wear rate obtained among the investigated alloys. Relative to the as-cast condition, the mass loss decreased by approximately 52.2%, while the wear rate and COF decreased by 55.7% and 22.6%, respectively. Compared with the solution-treated alloy, S3 exhibited further reductions of 37.3% in mass loss, 42.2% in wear rate, and 14.3% in COF. The superior wear resistance of S3 can be attributed to precipitation hardening associated with the formation of fine and uniformly distributed Al2Cu precipitates, increased hardness, refined eutectic silicon morphology, reduced microstrain, and lower dislocation density. These microstructural characteristics effectively improve the resistance of the alloy surface to abrasive and adhesive wear mechanisms.

In contrast, the over-aged alloy (S4) exhibited intermediate tribological behavior, with a mass loss of 11.8 mg, a wear rate of 2.96 × 10^{-4} mm^3/N·m, and a coefficient of friction of 0.52. According to Eq. 1, the increase in mass loss relative to S3 resulted in a corresponding increase in wear rate. Although these values remained superior to those of S1 and S2, they were inferior to those obtained for S3. Relative to the T6-treated condition, the mass loss increased by approximately 32.6%, while the wear rate and COF increased by 37.7% and 8.3%, respectively. This deterioration in wear performance can be explained by precipitate coarsening during prolonged aging, which weakens the precipitation strengthening effect and decreases the ability of the alloy surface to resist material removal. The tribological results indicate that the wear resistance followed the sequence: S3 (T6-treated) > S4 (Over-aged) > S2 (Solution-treated) > S1 (As-cast), whereas the coefficient of friction followed the reverse order: S1 > S2 > S4 > S3. These findings confirm that the T6 heat-treatment condition provides the optimum combination of wear resistance and frictional stability through the combined effects of precipitation strengthening, microstructural refinement, enhanced hardness, and improved crystallographic quality.

Fig. 6 presents the simultaneous variations in wear rate and coefficient of friction (COF) of the aluminum piston alloys under different heat-treatment conditions. The figure clearly illustrates a progressive reduction in both wear rate and friction coefficient from the as-cast condition to the T6-treated condition, followed by a slight increase after over-aging. The high mass loss of S1, when substituted into Eq. 1, yielded the highest wear rate (4.85 × 10^{-4} mm^3/N·m), whereas the minimum mass loss of S3 generated the lowest wear rate (2.15 × 10^{-4} mm3/N·m). The T6-treated sample also exhibited the smallest COF (0.48), confirming the effectiveness of precipitation strengthening and microstructural refinement in minimizing both material loss and frictional resistance. Although the over-aged sample (S4) retained better tribological properties than S1 and S2, its wear rate (2.96 × 10-4 mm3/N·m) and COF (0.52) increased relative to S3 because of precipitate coarsening and the reduced efficiency of the strengthening precipitates [24].

Table 3. Wear parameters of aluminum piston alloys subjected to different heat-treatment conditions.

Sample	Mass Loss (mg)	Wear Rate (×10^{-4} mm^3/N·m)	Coefficient of Friction (COF)
S1 (As-cast)	18.6	4.85	0.62
S2 (Solution-treated)	14.2	3.72	0.56
S3 (T6-treated)	8.9	2.15	0.48
S4 (Over-aged)	11.8	2.96	0.52

*Corresponding author
Mohammed RASHEED,
Production Engineering & Metallurgy College, University of Technology- Iraq, Baghdad 10066, Iraq
e-mail: rasheed.mohammed40@yahoo.com

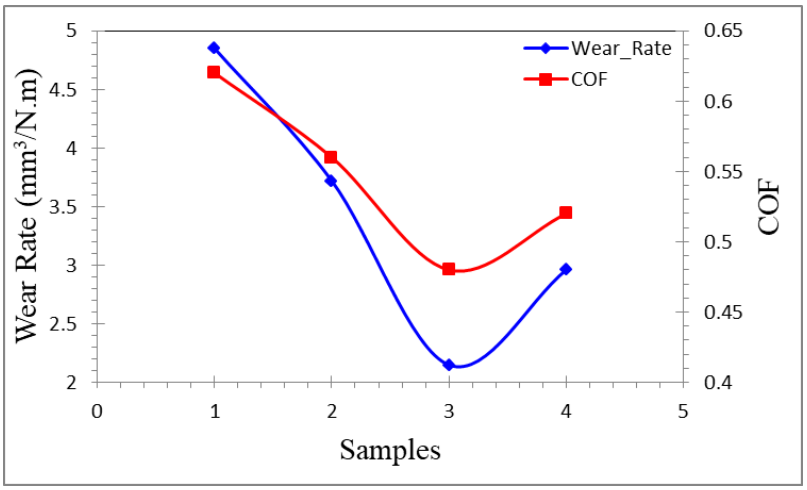

Fig. 6. Variation of wear rate and coefficient of friction (COF) of aluminum piston alloys subjected to different heat-treatment conditions: S1 (as-cast), S2 (solution-treated), S3 (T6-treated), and S4 (over-aged). The wear rate values were calculated according to Eq. (14). The T6-treated alloy exhibited the lowest wear rate and friction coefficient owing to precipitation hardening, refined eutectic silicon morphology, and enhanced hardness, whereas the as-cast alloy showed the highest wear rate and COF because of its coarse microstructure and greater susceptibility to abrasive and adhesive wear.

IMPACT STRENGTH

Fig. 7 presents Fig. 7 presents the impact strength behavior of the aluminum piston alloys subjected to different heat-treatment conditions, namely S1 (as-cast), S2 (solution-treated), S3 (T6-treated), and S4 (over-aged). The impact properties were evaluated using the Charpy impact test according to ASTM E23 to assess the ability of the alloys to absorb energy under sudden loading conditions. Since automotive pistons are continuously exposed to dynamic stresses and shock loads during engine operation, impact toughness is an important indicator of service reliability and resistance to catastrophic failure.

The impact strength values were calculated using the following equation [25]:

$$\text{Impact strength} = \frac{(\text{F.E.})}{(\text{d} \times \text{w})} \times 1000 \quad (2)$$

where F. E. is the absorbed fracture energy (J), d is the specimen thickness beneath the notch (mm), and w is the width of the remaining cross-sectional area (mm). As illustrated in Fig. 7, the as-cast alloy (S1) exhibited the lowest impact strength of 85 kJ/m2. The relatively poor toughness of S1 can be attributed to its coarse dendritic α-Al matrix, irregular eutectic silicon morphology, and the presence of casting defects such as porosity and microsegregation. These microstructural features act as stress concentration sites that facilitate crack initiation and accelerate crack propagation during impact loading, thereby reducing the resistance of the alloy to sudden fracture.

Following solution treatment, the impact resistance improved significantly. The S2 sample exhibited an impact strength of 102 kJ/m^2, representing an improvement of approximately 20.0% compared with the as-cast condition. This enhancement is associated with the dissolution of soluble intermetallic phases, homogenization of the aluminum matrix, and partial spheroidization of eutectic silicon particles during solution treatment. The reduction in microstructural heterogeneity promoted more uniform plastic deformation and improved crack resistance.

The highest impact performance was observed for the T6-treated alloy (S3), which exhibited an impact strength of 134 kJ/m2, as shown in Fig. 7. Compared with the as-cast alloy, the impact strength increased by approximately 57.6%, while an improvement of approximately 31.4% was achieved relative to the solution-treated sample. The superior impact resistance of S3 can be attributed to the formation of fine and uniformly distributed Al2Cu precipitates during artificial aging, together with the refinement and spheroidization of eutectic silicon particles. These microstructural modifications improve stress distribution throughout the matrix, delay crack initiation, and impede crack propagation, thereby enhancing the alloy's toughness. The excellent impact performance of S3 is also consistent with its superior crystallographic characteristics,

*Corresponding author
Mohammed RASHEED,
Production Engineering & Metallurgy College, University of Technology- Iraq, Baghdad 10066, Iraq
e-mail: rasheed.mohammed40@yahoo.com

including lower microstrain, reduced dislocation density, and larger crystallite size observed in the XRD analysis.

In contrast, the over-aged sample (S4) exhibited an impact strength of 116 kJ/m2. Although this value remained higher than those obtained for S1 and S2, it was approximately 13.4% lower than that of the T6-treated alloy. Compared with the as-cast condition, however, S4 still demonstrated an improvement of approximately 36.5% in impact strength. The reduction in impact resistance relative to S3 is attributed to precipitate coarsening during prolonged aging. As the strengthening precipitates grow and lose coherency with the matrix, their effectiveness in resisting crack propagation diminishes, leading to a reduction in toughness. Nevertheless, the more homogeneous microstructure of S4 still provided better impact resistance than the as-cast alloy.

The impact resistance trend observed in Fig. 7 can therefore be summarized as: S3 > S4 > S2 > S1

This sequence clearly demonstrates that the T6 heat-treatment condition provides the optimum balance between toughness and strength among the investigated aluminum piston alloys. The excellent performance of S3 highlights the beneficial role of precipitation hardening and microstructural refinement in improving crack resistance under dynamic loading conditions. In contrast, the inferior behavior of S1 reflects the detrimental influence of casting defects and coarse eutectic silicon particles, whereas the moderate performance of S4 indicates that excessive aging leads to a partial loss of the strengthening effect. These findings are in excellent agreement with the hardness measurements, tensile properties, microstructural observations, and XRD analyses presented in the previous sections, confirming that controlled heat treatment is an effective approach for enhancing the impact performance and overall mechanical reliability of aluminum piston alloys intended for automotive piston applications [26].

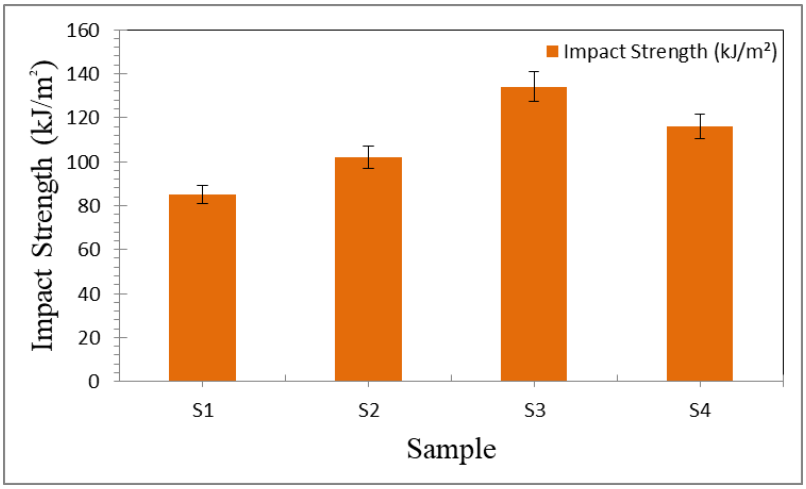

Fig. 7. Impact strength of S1 (as-cast), S2 (solution-treated), S3 (T6-treated), and S4 (over-aged) aluminum piston alloys measured according to ASTM E23.

FATIGUE PERFORMANCE

Fig. 8 and Table 4 present the fatigue behavior of the aluminum piston alloys subjected to different heat-treatment conditions, namely S1 (as-cast), S2 (solution-treated), S3 (T6-treated), and S4 (over-aged). Fatigue resistance is one of the most important mechanical properties for piston materials because pistons experience repeated thermal and mechanical stresses during engine operation. These cyclic loads promote the initiation and propagation of microscopic cracks that eventually lead to failure. Therefore, understanding the influence of heat treatment on fatigue performance is essential for improving the durability and service life of aluminum piston alloys. The fatigue behavior of the investigated samples was evaluated using rotating bending fatigue tests in accordance with ASTM E466. The relationship between the applied stress amplitude and the corresponding number of cycles to failure was described using Basquin's equation [27]:

$$\sigma_a = \sigma'f\,(2Nf)^b \quad (3)$$

where σ_a is the stress amplitude (MPa), $\sigma'f$ is the fatigue strength coefficient (MPa), Nf is the number of cycles to failure, and b is the fatigue strength exponent. Taking the logarithm of both sides yields [28]:

*Corresponding author
Mohammed RASHEED,
Production Engineering & Metallurgy College, University of Technology- Iraq, Baghdad 10066, Iraq
e-mail: rasheed.mohammed40@yahoo.com

$$\log \sigma_a = \log \sigma'f + b \log(2Nf) \quad (4)$$

This equation forms the basis for constructing the S–N curves shown in Fig. 8 and allows the fatigue performance of the different heat-treatment conditions to be quantitatively compared.

As illustrated in Table 4 and Fig. 8, the as-cast alloy (S1) exhibited the poorest fatigue performance among all investigated samples. At a stress amplitude of 140 MPa, failure occurred after only 2.0 × 104 cycles, while reducing the stress amplitude to 120 MPa and 100 MPa extended the fatigue life to 5.0 × 104 and 9.0 × 104 cycles, respectively. The fatigue limit of S1 was approximately 90 MPa, corresponding to a fatigue life of 1.2 × 105 cycles. The relatively short fatigue life of S1 can be attributed to the coarse dendritic α-Al matrix, irregular eutectic silicon particles, and the presence of casting defects such as porosity and microshrinkage. These microstructural imperfections act as stress concentration sites, facilitating early crack initiation and rapid crack propagation under cyclic loading.

Following solution treatment, a noticeable improvement in fatigue resistance was observed. The S2 sample sustained a stress amplitude of 160 MPa for 4.0 × 104 cycles, while fatigue lives of 9.0 × 104, 1.8 × 105, and 2.5 × 105 cycles were achieved at stress amplitudes of 140 MPa, 120 MPa, and 110 MPa, respectively. Compared with the as-cast alloy, the fatigue limit increased from 90 MPa to 110 MPa, representing an improvement of approximately 22.2%. Moreover, the fatigue life at the fatigue limit increased by approximately 108%, from 1.2 × 105 cycles in S1 to 2.5 × 105 cycles in S2. This enhancement is associated with the dissolution of segregated phases and homogenization of the matrix during solution treatment, which reduced local stress concentrations and delayed crack initiation.

The most significant enhancement in fatigue performance was achieved for the T6-treated alloy (S3). As shown in Fig. 8, S3 sustained the highest stress amplitudes while maintaining the longest fatigue lives. At a stress amplitude of 190 MPa, the alloy survived for 1.2 × 105 cycles, while reducing the stress amplitude to 170 MPa and 155 MPa increased the fatigue life to 2.8 × 105 and 4.9 × 105 cycles, respectively. The fatigue limit of S3 reached approximately 145 MPa, corresponding to a fatigue life of 6.8 × 105 cycles. Relative to the as-cast condition, the fatigue limit increased by approximately 61.1%, whereas the fatigue life improved by approximately 467%. Compared with the solution-treated alloy, S3 exhibited improvements of approximately 31.8% in fatigue limit and 172% in fatigue life. The superior fatigue resistance of S3 can be attributed to the precipitation hardening effect associated with fine and uniformly distributed Al2Cu precipitates formed during artificial aging. In addition, the refinement and spheroidization of eutectic silicon particles, increased crystallite size, reduced microstrain, and lower dislocation density observed in the XRD analysis contributed significantly to delaying crack nucleation and retarding crack growth during cyclic loading.

In contrast, the over-aged alloy (S4) exhibited intermediate fatigue behavior between S2 and S3. The sample endured 8.0 × 104 cycles at a stress amplitude of 175 MPa, while fatigue lives of 1.9 × 105, 3.1 × 105, and 4.2 × 105 cycles were recorded at stress amplitudes of 155 MPa, 135 MPa, and 125 MPa, respectively. The fatigue limit of S4 was approximately 125 MPa, which remained substantially higher than those of S1 and S2 but was lower than that of S3. Compared with the T6-treated alloy, the fatigue limit decreased by approximately 13.8%, while the fatigue life decreased by approximately 38.2%. Nevertheless, relative to the as-cast condition, S4 still exhibited improvements of approximately 38.9% in fatigue limit and 250% in fatigue life. The deterioration in fatigue resistance compared with S3 is mainly attributed to precipitate coarsening during prolonged aging, which reduces the effectiveness of precipitation strengthening and facilitates crack propagation.

The S–N curves shown in Fig. 8 clearly demonstrate that increasing the number of cycles to failure requires a reduction in the applied stress amplitude for all investigated samples, which is characteristic of metallic fatigue behavior. The T6-treated alloy consistently occupied the upper region of the S–N diagram, indicating superior resistance to cyclic loading, whereas the as-cast alloy remained in the lower region, reflecting its susceptibility to premature fatigue failure. The solution-treated and over-aged alloys exhibited intermediate behavior, highlighting the beneficial influence of heat treatment and the detrimental effect of excessive aging.

The fatigue resistance of the investigated aluminum piston alloys followed the sequence: S3 > S4 > S2 > S1. This trend confirms that the T6 heat-treatment condition provides the optimum fatigue performance and the longest service life among the investigated alloys. The outstanding behavior of S3 is consistent with the

*Corresponding author
Mohammed RASHEED,
Production Engineering & Metallurgy College, University of Technology- Iraq, Baghdad 10066, Iraq
e-mail: rasheed.mohammed40@yahoo.com

hardness measurements, tensile properties, impact strength results, microstructural observations, and XRD analyses presented in the previous sections. These findings demonstrate that optimized precipitation hardening, eutectic silicon refinement, and improved crystallographic quality are the primary factors responsible for enhancing the fatigue performance of aluminum piston alloys intended for automotive piston applications [28].

Table 4. Fatigue properties of aluminum piston alloys under different heat-treatment conditions.

Sample	Stress Amplitude (MPa)	Number of Cycles to Failure, Nf
S1	140	2.0×10^4
S1	120	5.0×10^4
S1	100	9.0×10^4
S1	90	1.2×10^5
S2	160	4.0×10^4
S2	140	9.0×10^4
S2	120	1.8×10^5
S2	110	2.5×10^5
S3	190	1.2×10^5
S3	170	2.8×10^5
S3	155	4.9×10^5
S3	145	6.8×10^5
S4	175	8.0×10^4
S4	155	1.9×10^5
S4	135	3.1×10^5
S4	125	4.2×10^5

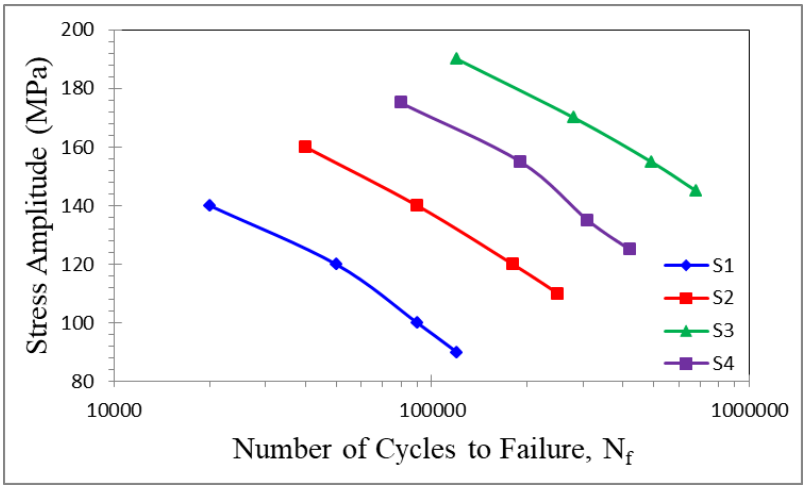

Fig. 8. S–N curves of S1 (as-cast), S2 (solution-treated), S3 (T6-treated), and S4 (over-aged) aluminum piston alloys obtained from rotating bending fatigue tests according to ASTM E466.

FRACTOGRAPHY (FESEM)

Fig. 9 presents the FESEM fractographs of the fractured aluminum piston alloys subjected to different heat-treatment conditions, namely (a) S1 (as-cast), (b) S2 (solution-treated), (c) S3 (T6-treated), and (d) S4 (over-aged). The fracture surfaces were examined at a magnification of 20.00 k× using a ZEISS FESEM operated at an accelerating voltage of 10.00 kV, with a working distance of 6.8 mm and a scale bar of 200 nm. The FESEM analysis provides valuable information regarding the dominant fracture mechanisms and reveals how thermal processing modifies crack initiation and propagation behavior. Significant differences in the fracture morphology were observed among the investigated samples, which correlate well with the hardness, tensile, impact, and fatigue properties discussed in the previous sections.

*Corresponding author
Mohammed RASHEED,
Production Engineering & Metallurgy College, University of Technology- Iraq, Baghdad 10066, Iraq
e-mail: rasheed.mohammed40@yahoo.com

The fracture surface of the as-cast alloy (S1), shown in Fig. 9(a), exhibited a predominantly brittle fracture mode characterized by large cleavage facets, numerous fractured eutectic silicon particles, microcracks, and localized porosity. The cleavage planes appeared relatively flat and angular, indicating limited plastic deformation before failure. The presence of fractured acicular silicon particles suggests that these particles acted as stress concentration sites that promoted crack nucleation. Furthermore, the observed porosity and microcracks provided preferential pathways for crack propagation, resulting in premature fracture. These fractographic characteristics explain the inferior mechanical performance of S1, which exhibited the lowest hardness, the lowest tensile strength, the lowest impact strength (85 kJ/m2), and the shortest fatigue life (1.2 × 105 cycles). Therefore, the as-cast condition was the most susceptible to catastrophic failure under both static and cyclic loading.

Following solution treatment, substantial changes in fracture morphology were observed. The S2 sample, shown in Fig. 9(b), exhibited a mixed-mode fracture characterized by the presence of numerous shallow dimples, dispersed microvoids, and spheroidized eutectic silicon particles. Compared with S1, the cleavage regions became less pronounced, while the density of ductile features increased significantly. The shallow dimples indicate that the alloy underwent greater plastic deformation before fracture. The spheroidization of silicon particles reduced the sharp edges that previously acted as crack initiators in the as-cast condition. Consequently, S2 exhibited improved mechanical properties, including higher hardness, increased tensile strength, enhanced impact resistance (102 kJ/m2), and a longer fatigue life (2.5 × 105 cycles) than S1. These observations confirm that solution treatment effectively reduced microstructural heterogeneity and improved crack resistance.

The most remarkable fracture characteristics were observed for the T6-treated alloy (S3), as shown in Fig. 9(c). The fracture surface was dominated by a large population of fine, deep, and uniformly distributed dimples, accompanied by only a limited number of fractured silicon particles. The dimple morphology is characteristic of a ductile fracture mechanism governed by microvoid nucleation, growth, and coalescence. Compared with S1 and S2, the dimples in S3 were deeper, finer, and more homogeneous, indicating extensive plastic deformation and superior energy absorption capability prior to failure. The absence of large cleavage facets and the reduction in fractured silicon particles suggest that the crack propagation resistance was substantially enhanced. The improved fracture behavior of S3 is directly associated with the precipitation of fine and uniformly distributed Al2Cu particles during artificial aging, which strengthened the aluminum matrix while maintaining adequate ductility. These fractographic observations correlate well with the superior mechanical performance of S3, which exhibited the highest hardness, the maximum ultimate tensile strength (265 MPa), the highest impact strength (134 kJ/m2), and the longest fatigue life (6.8 × 105 cycles). Therefore, the T6-treated alloy demonstrated the optimum balance between strength, toughness, and fracture resistance.

In contrast, the over-aged alloy (S4), illustrated in Fig. 9(d), exhibited fracture characteristics intermediate between those of S2 and S3. Although ductile dimples remained the dominant feature, their size increased and their distribution became less uniform compared with the T6-treated condition. In addition, localized cleavage facets and coarse fractured precipitates were clearly observed. The appearance of these coarse precipitates indicates that prolonged aging promoted precipitate coarsening, thereby reducing the effectiveness of precipitation strengthening. The coexistence of ductile and brittle features suggests a mixed fracture mechanism. Compared with S3, the fracture resistance of S4 deteriorated, which is consistent with the reductions observed in impact strength (116 kJ/m2) and fatigue life (4.2 × 105 cycles). Nevertheless, S4 still exhibited a more ductile fracture morphology than the as-cast alloy, explaining its superior mechanical performance relative to S1.

A comparison of the four FESEM fractographs clearly demonstrates that thermal processing significantly altered the fracture mechanisms of the aluminum piston alloys. The fracture mode progressively evolved from a predominantly brittle cleavage fracture in the as-cast condition to a ductile microvoid coalescence fracture after optimized T6 treatment. Specifically, the number of cleavage facets, fractured silicon particles, and secondary cracks decreased in the order: S1 > S4 > S2 > S3, whereas the density and uniformity of ductile dimples increased according to: S3 > S4 > S2 > S1. Similarly, the resistance to crack initiation and propagation followed the sequence: S3 > S4 > S2 > S1, which is in excellent agreement with the trends observed in hardness measurements, tensile properties, impact strength, and fatigue performance.

*Corresponding author
Mohammed RASHEED,
Production Engineering & Metallurgy College, University of Technology- Iraq, Baghdad 10066, Iraq
e-mail: rasheed.mohammed40@yahoo.com

The FESEM fractographic analysis confirms that the superior mechanical properties of the T6-treated alloy originated from the synergistic effects of eutectic silicon refinement, homogeneous precipitation strengthening, and reduced defect density. In contrast, the poor fracture behavior of the as-cast alloy was primarily associated with casting defects, coarse silicon particles, and brittle crack propagation pathways. The over-aged condition retained moderate fracture resistance but suffered from precipitate coarsening, whereas solution treatment provided intermediate improvements through matrix homogenization and silicon spheroidization. These findings demonstrate that optimized T6 heat treatment is the most effective processing route for improving the fracture resistance and overall reliability of aluminum piston alloys intended for automotive piston applications [29, 30].

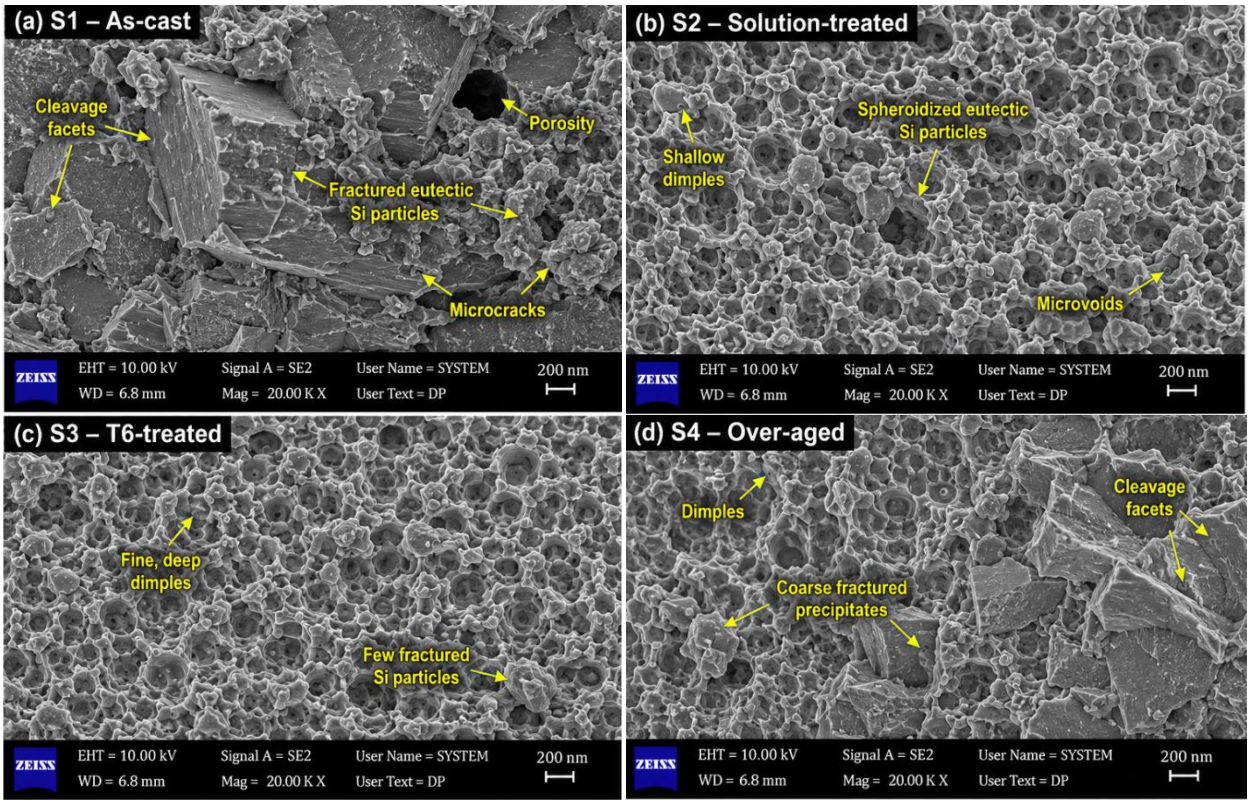

Fig. 9. FESEM fractographs of fractured aluminum piston alloys under different heat-treatment conditions recorded at 20.00 k× magnification with a 200 nm scale bar: (a) S1 (as-cast), showing cleavage facets, fractured eutectic silicon particles, microcracks, and porosity; (b) S2 (solution-treated), exhibiting shallow dimples, microvoids, and spheroidized silicon particles; (c) S3 (T6-treated), characterized by fine and deep dimples with limited fractured silicon particles, indicating ductile microvoid coalescence; and (d) S4 (over-aged), displaying mixed fracture features consisting of ductile dimples, cleavage facets, and coarse fractured precipitates. The T6-treated alloy exhibited the highest fracture resistance, whereas the as-cast alloy showed the most brittle fracture behavior.

COMPARATIVE DISCUSSION AMONG S1–S4

The results obtained from the microstructural characterization, X-ray diffraction analysis, hardness measurements, tensile testing, impact evaluation, fatigue assessment, and fractographic observations collectively demonstrate that the mechanical performance of aluminum piston alloys is strongly dependent on the applied heat-treatment condition. The four investigated samples exhibited distinctly different responses owing to variations in eutectic silicon morphology, precipitation behavior, crystallographic characteristics, and defect distribution. A comprehensive comparison among S1 (as-cast), S2 (solution-treated), S3 (T6-treated), and S4 (over-aged) provides a clearer understanding of the strengthening mechanisms governing the performance of aluminum piston alloys intended for automotive piston applications.

*Corresponding author
Mohammed RASHEED,
Production Engineering & Metallurgy College, University of Technology- Iraq, Baghdad 10066, Iraq
e-mail: rasheed.mohammed40@yahoo.com

The as-cast alloy (S1) consistently exhibited the poorest performance in all investigated properties. Optical microscopy and SEM analyses revealed a coarse dendritic α-Al matrix containing irregular and acicular eutectic silicon particles together with casting defects such as porosity and microsegregation. These microstructural features promoted stress localization and facilitated crack initiation. XRD analysis further confirmed that S1 possessed the smallest average crystallite size (28.05 nm), the highest microstrain values (2.63–4.89 × 10-3), and the highest dislocation density values (1.17–1.39 × 10-3 nm-2), indicating the presence of considerable lattice distortion and crystallographic imperfections. Consequently, S1 exhibited the lowest hardness, the minimum tensile properties (YS = 128 MPa, UTS = 185 MPa, and elongation = 4.8%), the lowest impact strength (85 kJ/m²), and the shortest fatigue life (1.2 × 105 cycles). The FESEM fractographs also showed extensive cleavage facets, fractured silicon particles, porosity, and microcracks, confirming that brittle fracture dominated the failure mechanism in the as-cast condition.

The solution-treated alloy (S2) demonstrated moderate improvements in both structural and mechanical properties. The solution treatment promoted the dissolution of segregated phases and partial spheroidization of eutectic silicon particles, resulting in a more homogeneous matrix. The average crystallite size increased to approximately 31.00 nm, while the microstrain and dislocation density values decreased compared with S1. These structural modifications translated into enhanced mechanical behavior, as evidenced by increases in tensile properties (YS = 145 MPa, UTS = 210 MPa, and elongation = 6.2%). Relative to S1, the yield strength and ultimate tensile strength increased by approximately 13.3% and 13.5%, respectively, whereas elongation improved by 29.2%. Similarly, the impact strength increased from 85 kJ/m2 to 102 kJ/m2, representing an enhancement of approximately 20.0%, while the fatigue life increased from 1.2 × 105 cycles to 2.5 × 105 cycles. The FESEM observations revealed shallow dimples and microvoids, indicating a transition from predominantly brittle fracture toward a mixed ductile–brittle failure mode.

Among all investigated conditions, the T6-treated alloy (S3) exhibited the most favorable combination of structural integrity and mechanical performance. Artificial aging following solution treatment promoted the precipitation of fine and uniformly distributed Al_2Cu particles, which effectively impeded dislocation movement and strengthened the aluminum matrix. XRD analysis showed that S3 possessed the largest average crystallite size (37.27 nm), the lowest microstrain values (1.93–3.81 × 10-3), the lowest dislocation density (0.66–0.78 × 10-3 nm-2), and the highest texture coefficient values reaching 1.21, indicating superior crystallographic quality and enhanced preferred orientation. These favorable structural characteristics resulted in the highest hardness among the investigated samples and produced exceptional tensile properties (YS = 182 MPa, UTS = 265 MPa, and elongation = 7.1%). Compared with the as-cast alloy, the yield strength increased by approximately 42.2%, the ultimate tensile strength improved by 43.2%, and the elongation increased by 47.9%. Furthermore, S3 exhibited the highest impact strength (134 kJ/m2), corresponding to an improvement of 57.6% relative to S1, and demonstrated the longest fatigue life (6.8 × 105 cycles), which was approximately 467% higher than that of the as-cast alloy. The FESEM fractographs were dominated by fine and deep equiaxed dimples, reflecting extensive plastic deformation and excellent resistance to crack propagation. These results confirm that the T6 treatment provides the optimum balance between strength, toughness, and durability.

The over-aged alloy (S4) exhibited intermediate behavior between S2 and S3. Although prolonged aging resulted in precipitate coarsening, the microstructure remained more homogeneous than that of the as-cast condition. The average crystallite size decreased slightly to approximately 32.12 nm, accompanied by moderate increases in microstrain and dislocation density compared with S3. Consequently, the tensile properties decreased to YS = 158 MPa, UTS = 232 MPa, and elongation = 5.9%, although these values remained higher than those of S1 and S2. The impact strength reached 116 kJ/m2, which was approximately 36.5% higher than that of the as-cast alloy but 13.4% lower than that of S3. Similarly, the fatigue life decreased to 4.2 × 105 cycles, representing a reduction of approximately 38.2% compared with the T6-treated condition. FESEM analysis revealed mixed fracture characteristics consisting of dimples, localized cleavage facets, and coarse fractured precipitates, indicating that precipitate coarsening reduced the effectiveness of precipitation strengthening and crack-arrest mechanisms.

A direct comparison of the investigated samples clearly demonstrates that the strengthening mechanisms evolved significantly with thermal processing. The mechanical performance rankings for the investigated properties can be summarized as follows:

- Hardness: S3 > S4 > S2 > S1

*Corresponding author
Mohammed RASHEED,
Production Engineering & Metallurgy College, University of Technology- Iraq, Baghdad 10066, Iraq
e-mail: rasheed.mohammed40@yahoo.com

- Yield Strength: S3 > S4 > S2 > S1
- Ultimate Tensile Strength: S3 > S4 > S2 > S1
- Elongation: S3 > S2 > S4 > S1
- Impact Strength: S3 > S4 > S2 > S1
- Fatigue Life: S3 > S4 > S2 > S1
- Crack Resistance: S3 > S4 > S2 > S1

These trends indicate that the improvements in mechanical behavior are closely related to microstructural refinement, crystallographic perfection, and optimized precipitation hardening. Solution treatment alone effectively homogenized the matrix and improved ductility, whereas artificial aging produced fine precipitates that maximized strengthening efficiency. However, excessive aging promoted precipitate coarsening, thereby reducing the beneficial effects of precipitation hardening.

The comparative analysis confirms that the T6 heat-treatment condition (S3) represents the optimum processing route for aluminum piston alloys, providing the best balance among hardness, tensile strength, ductility, impact toughness, fatigue resistance, and fracture behavior. The superior performance of S3 highlights the critical role of controlled thermal processing in enhancing the reliability and service life of aluminum pistons used in automotive engines. These findings provide valuable guidance for selecting suitable heat-treatment strategies and contribute to the future design and optimization of high-performance aluminum piston alloys.

CONCLUSION

In this study, a comprehensive comparative investigation was conducted to evaluate the influence of different heat-treatment conditions on the microstructural evolution, crystallographic characteristics, and mechanical performance of aluminum piston alloys intended for automotive applications. Four representative conditions were examined, namely S1 (as-cast), S2 (solution-treated), S3 (T6-treated), and S4 (over-aged). The results demonstrated that thermal processing plays a decisive role in modifying the structural integrity and service performance of aluminum piston alloys. Microstructural analyses revealed that the as-cast alloy possessed a coarse dendritic α-Al matrix with irregular eutectic silicon particles and casting defects, whereas solution treatment promoted matrix homogenization and partial spheroidization of silicon particles. The T6-treated alloy exhibited the most refined microstructure with uniformly distributed strengthening precipitates, while the over-aged condition resulted in precipitate coarsening. XRD analysis confirmed that the T6-treated sample showed the largest average crystallite size (37.27 nm), the lowest microstrain (1.93–3.81 × 10-3), and the lowest dislocation density (0.66–0.78 × 10-3 nm-2), indicating superior crystallographic quality. Mechanical testing demonstrated that the T6-treated alloy exhibited the optimum combination of properties, including the highest yield strength (182 MPa), ultimate tensile strength (265 MPa), elongation (7.1%), impact strength (134 kJ/m2), and fatigue life (6.8×10^5 cycles). Compared with the as-cast condition, the T6 treatment improved the yield strength, ultimate tensile strength, impact strength, and fatigue life by approximately 42.2%, 43.2%, 57.6%, and 467%, respectively. In contrast, the over-aged alloy showed moderate reductions in performance due to precipitate coarsening, although it still outperformed the as-cast condition. FESEM fractographic analysis further confirmed a transition from brittle fracture characterized by cleavage facets and fractured silicon particles in S1 to a predominantly ductile microvoid coalescence mechanism in S3. The results establish that the T6 heat-treatment condition provides the most favorable balance between strength, ductility, toughness, and fatigue resistance. Therefore, optimized T6 processing represents an effective strategy for enhancing the durability, reliability, and service life of aluminum piston alloys used in high-performance automotive engine components. The findings of this study provide valuable guidelines for heat-treatment selection and future alloy optimization in advanced piston manufacturing.

REFERENCES

[1] R. Almeida Rodrigues, A. da Silva, and J. P. Costa, “Effect of different T6 heat treatment conditions on the microstructural and mechanical behavior of A356 aluminum alloy,” *Metals*, vol. 15, no. 7, p. 692, 2025. https://doi.org/10.3390/met15070692

*Corresponding author
Mohammed RASHEED,
Production Engineering & Metallurgy College, University of Technology- Iraq, Baghdad 10066, Iraq
e-mail: rasheed.mohammed40@yahoo.com

[2] F. E. El Garchani and M. R. Kabiri, "The study on characteristics of heat treatment of the AA2024 aluminum alloys," *J. Multidiscip. Appl. Nat. Sci.*, vol. 3, no. 2, pp. 122–130, 2023. https://doi.org/10.47352/jmans.2774-3047.166
[3] H. Rivera-Cerezo et al., "Effect of heat treatment on the electrochemical behavior of aluminum alloys," *Metals*, vol. 13, no. 3, p. 429, 2023. https://doi.org/10.3390/met13030429
[4] M. M. Khalilabad et al., "Effect of heat treatments on microstructural and mechanical properties of aluminum alloys," *Mater. Sci. Eng. A*, vol. 832, p. 142431, 2022. https://doi.org/10.1016/j.msea.2021.142431
[5] N. Kumar, T. N. Shashank, and D. Dhruthi, "Different ceramic reinforcements in aluminium metal matrix composites: A review," *ECS J. Solid State Sci. Technol.*, vol. 10, no. 5, p. 053003, 2021. https://doi.org/10.1149/2162-8777/ac0114
[6] V. Vivekanandam, S. S. Joshi, J. Lazaro-Nebreda, and Z. Fan, "Effect of processing-induced oxides on the fatigue life variability of 6082 Al-Mg-Si alloy extruded components," *J. Manuf. Mater. Process.*, vol. 9, no. 7, p. 247, 2025. https://doi.org/10.3390/jmmp9070247
[7] M. G. Mahmoud et al., "Influence of praseodymium additions and multiple-step T6 on microstructure and mechanical properties of 7075 alloy," *Int. J. Metalcasting*, 2025. https://doi.org/10.1007/s40962-025-01728-y
[8] P. Huang et al., "Achieving highly dense metal injection moulding 6061 Al with superior strength–ductility," *Mater. Sci. Eng. A*, vol. 931, p. 148827, 2025. https://doi.org/10.1016/j.msea.2025.148827
[9] Y. Li et al., "Optimizing aluminum content in DZ409 alloy: Analysis of microstructural and mechanical properties," *Metals*, vol. 14, no. 6, p. 621, 2024. https://doi.org/10.3390/met14060621
[10] M. Naveed et al., "Effect of heat treatment on sliding wear resistance of hybrid aluminum matrix composites," *Recent Prog. Mater.*, vol. 5, no. 2, 2023. https://doi.org/10.21926/rpm.2302015
[11] M. Moy et al., "Influence of heat treatment on the microstructure, texture and formability of 2024 aluminium alloy," *Mater. Sci. Eng. A*, vol. 552, pp. 48–60, 2012. https://doi.org/10.1016/j.msea.2012.04.113
[12] M. Millett et al., "The effect of heat treatment on the shock induced mechanical properties of aluminium alloy 7017," *Scr. Mater.*, vol. 51, no. 10, pp. 967–972, 2004. https://doi.org/10.1016/j.scriptamat.2004.07.020
[13] H. Paulisch et al., "Microstructural evolution during heat treatment of aluminum alloys," *Mater. Sci. Eng. A*, vol. 628, pp. 133–142, 2015. https://doi.org/10.1016/j.msea.2014.12.040
[14] J. Hirsch, "Recent development in aluminium for automotive applications," *Trans. Nonferrous Met. Soc. China*, vol. 24, no. 7, pp. 1995–2002, 2014. https://doi.org/10.1016/S1003-6326(14)63305-7
[15] J. Hirsch, "Aluminium in innovative light-weight car design," *Mater. Trans.*, vol. 52, no. 5, pp. 818–824, 2011. https://doi.org/10.2320/matertrans.L-MZ201132
[16] D. Emadi, J. Gruzleski, J. Closset, and L. F. Lafrance, *Principles of Metal Casting*. Elsevier, 2021. https://doi.org/10.1016/B978-0-12-824980-3.00001-8
[17] L. Lu, A. K. Dahle, and D. H. StJohn, "The role of silicon morphology in aluminum casting alloys," *JOM*, vol. 57, no. 11, pp. 48–52, 2005. https://doi.org/10.1007/s11837-005-0234-3
[18] M. Tiryakioğlu, "The effect of porosity on fatigue properties of cast aluminum alloys," *Mater. Sci. Eng. A*, vol. 506, pp. 168–173, 2009. https://doi.org/10.1016/j.msea.2008.11.041
[19] M. M. Tash et al., "Influence of heat treatment on wear behavior of Al–Si alloys," *Wear*, vol. 376–377, pp. 1520–1528, 2017. https://doi.org/10.1016/j.wear.2017.01.019
[20] S. Shivkumar, C. Keller, and D. Apelian, "Aging behavior in cast Al–Si–Mg alloys," *AFS Trans.*, vol. 98, pp. 905–911, 1990. https://doi.org/10.4271/900440
[21] M. Tash, A. Samuel, F. Mucciardi, and H. Doty, "Effect of solution heat treatment on eutectic silicon particles," *Mater. Charact.*, vol. 57, no. 4–5, pp. 275–292, 2006. https://doi.org/10.1016/j.matchar.2006.02.003
[22] M. A. Easton and D. H. StJohn, "An analysis of the relationship between grain size, microstructure and properties," *Metall. Mater. Trans. A*, vol. 36, pp. 1911–1920, 2005. https://doi.org/10.1007/s11661-005-0054-7
[23] J. Campbell, *Complete Casting Handbook*, 2nd ed. Oxford, U.K.: Elsevier, 2015. https://doi.org/10.1016/C2013-0-16374-3

*Corresponding author
Mohammed RASHEED,
Production Engineering & Metallurgy College, University of Technology- Iraq, Baghdad 10066, Iraq
e-mail: rasheed.mohammed40@yahoo.com

[24] A. M. Samuel, F. H. Samuel, and H. W. Doty, "Observations on the formation of Al_2Cu phases in aluminum alloys," *J. Mater. Sci.*, vol. 31, pp. 5529–5539, 1996. https://doi.org/10.1007/BF00355898
[25] M. Tiryakioğlu, "On fatigue crack initiation in cast aluminum alloys," *Int. J. Fatigue*, vol. 30, no. 9, pp. 1513–1518, 2008. https://doi.org/10.1016/j.ijfatigue.2007.11.009
[26] A. K. Dahle and D. H. StJohn, "The role of eutectic silicon in cast aluminum alloys," *Acta Mater.*, vol. 47, no. 1, pp. 31–41, 1999. https://doi.org/10.1016/S1359-6454(98)00228-6
[27] Y. Birol, "Response to T6 heat treatment of Sr-modified Al–Si casting alloys," *J. Alloys Compd.*, vol. 486, no. 1–2, pp. 219–222, 2009. https://doi.org/10.1016/j.jallcom.2009.06.177
[28] M. Zamani, M. Toschi, and A. Morri, "Fatigue behavior of heat-treated cast aluminum alloys," *Procedia Struct. Integr.*, vol. 26, pp. 58–65, 2020. https://doi.org/10.1016/j.prostr.2020.06.009
[29] Y. Zuo et al., "Microstructure evolution and mechanical properties of heat-treated Al–Si alloys," Materials, vol. 14, no. 21, p. 6454, 2021. https://doi.org/10.3390/ma14216454
[30] M. K. Surappa, "Aluminium matrix composites: Challenges and opportunities," Sadhana, vol. 28, no. 1–2, pp. 319–334, 2003. https://doi.org/10.1007/BF02717141.

*Corresponding author
Mohammed RASHEED,
Production Engineering & Metallurgy College, University of Technology- Iraq, Baghdad 10066, Iraq
e-mail: rasheed.mohammed40@yahoo.com